Document NWPSAF_EC_VS_026

Version 1.0

2/7/15

Microwave Surface Emissivity over sea-ice
Fabrizio Baordo and Alan Geer.

Microwave Surface Emissivity over sea-ice

Fabrizio Baordo[1] and Alan Geer[2]

[1] Bureau of Meteorology, Melbourne, Australia
[2] ECMWF, Reading, UK

This documentation was developed within the context of the EUMETSAT Satellite Application Facility on Numerical Weather Prediction (NWP SAF), under the Cooperation Agreement dated 29 June 2011, between EUMETSAT and the Met Office, UK, by one or more partners within the NWP SAF. The partners in the NWP SAF are the Met Office, ECMWF, KNMI and Météo France.

Change record			
Version	Date	Author / changed by	Remarks
1.0	2/7/15	F. Baordo and A. Geer	

NWP SAF Technical Report
Microwave surface emissivity over sea-ice

Visiting scientist mission, ECMWF, May-June 2015

Fabrizio Baordo
Bureau of Meteorology, Melbourne, Australia
Alan J. Geer
ECMWF, Reading, United Kingdom

ABSTRACT

The aim of this report is to investigate the existing FASTEM parametric models for microwave emissivity of sea-ice in order to evaluate the possibility of using them for satellite data assimilation over sea-ice in numerical weather prediction (NWP) systems. To guide our study we used measurements of emissivity derived from SSMIS observations. Results show that it is very difficult to prescribe an emissivity spectrum to a particular ice surface type and consequently it is not feasible to model the emissivity using only one FASTEM ice category which can be globally used across all the 19-183 GHz range. However, statistics of retrieved emissivities and analysis of first-guess departures (e.g. observation minus forecast differences) indicate that the choice of the FASTEM 'Compact' ice type might be a good approximation to adopt within NWP models for simulating temperature sounding observations. For frequencies above 150 GHz, the FASTEM model has not been found reliable: emissivity retrievals at 183±7 GHz are systematically larger than that predicted by the model at 183 GHz. That FASTEM emissivity is too low and this was also confirmed by the magnitude of the first-guess departures at 183±7 and 183±3 GHz which are constantly characterised by large positive biases. From the relationship between the SSMIS retrieved emissivities at 183±7 and 150 GHz it is possible to approximate the emissivity at 183 GHz as a linear function of the emissivity at 150 GHz. We derived a set of model coefficients which, according to the season and the polar region, can increase the FASTEM emissivities at 183 GHz from a minimum of 11% to a maximum of 35%. The linear approximation helps to improve the fit to the observations although the magnitude of the improvements clearly has a seasonal and geographical dependency. The results are generally promising and the next step is to verify the impact of using the linear model in data assimilation experiments.

1 Introduction

The ability to assimilate satellite observations over sea-ice regions is of particular importance to NWP models because of the scarcity of conventional data. The assimilation of microwave radiances sensitive to temperature and moisture is now well established over the ocean where surface emissivity models are very accurate. Satellite sounding over land has also become increasingly used thanks to the possibility of retrieving the emissivity directly from satellite measurements (e.g. Karbou et al., 2005) and the development of surface emissivity atlases (e.g. Aires et al., 2010). However, the use of monthly-mean emissivity climatology is not very suitable for fast-changing and dynamic surfaces such as sea-ice which drifts, deforms, melts or forms from day to day. The emissivity retrieval approach over sea-ice regions has been recently explored and it has in part allowed to extend the assimilation of the temperature and humidity microwave sounding channels (Karbou et al., 2014; Di Tomaso et al., 2013). However, the lower-peaking channels generally show large biases in first-guess departures which are most likely related to errors in the estimate of emissivity and skin temperature. The aim of this report is to better understand the variability of the ice emissivity in order to evaluate the reliability of the existing FASTEM models and, if possible, provide a better parametrisation. To guide our analysis, we use observations from SSMIS (F17) which is the only space instrument with polar coverage and the ability to measure

the surface and atmospheric signal across the 19-183 GHz range. For the purpose of our work, SSMIS observations over sea-ice have not been actively assimilated within the ECMWF Integrated forecasting System (IFS), but they have been only used to monitor the first-guess departures.

2   Modelling surface emissivity over sea-ice

The sea-ice emissivity is highly variable considering a quite large number of factors such as the ice density, the presence of an overlying layer of snow and the inclusion of brine and air pocket in the ice. In addition, the emissivity at a certain frequency, polarisation and incidence angle, is a function of surface scattering, subsurface extinction and reflection between layers with different permittivity. As a result, an accurate physical model for describing the sea-ice emissivity requires a large number of parameters which are not really available on the spatial and temporal scale of NWP models. An initial way to characterise the emissivity of an ice-affected ocean surface is to recognise the different spectral signature of ocean and ice. In a simple approximation, assuming a constant surface temperature, the sea-ice emissivity at a specific frequency v and incidence angle θ can be calculated as the contribution from the open water emissivity (ε_{ocean}) and the ice emissivity (ε_{ice}) weighted by the sea-ice concentration (C_{ice}):

$$\varepsilon(\theta, v) = (1 - C_{ice})\varepsilon_{ocean}(\theta, v) + C_{ice}\varepsilon_{ice}(\theta, v). \tag{1}$$

In the context of an NWP system, the sea-ice fraction is generally a parameter of the forecast model and the emissivity over ocean can be calculated from the accurate parametrisation available in RTTOV. Clearly, a good knowledge of the spectral variability of ε_{ice} is critical to minimise the error on the estimate of the emissivity over sea-ice. In the following sections, we explore the signature of the ice emissivity by looking at the existing parametric models which are part of the fast generic microwave emissivity model (FASTEM, English and Hewison, 1998) and comparing them to emissivities retrieved from SSMIS observations.

3   FASTEM ice emissivity models

Hewison and English (1999) used airborne microwave radiometer measurements obtained over the northern Baltic Sea, developed a parametric model based on dielectric permittivity and surface scattering which can represent the microwave spectra of different ice surfaces. Every surface category is parametrised by five coefficients which together with frequency, polarisation and incidence angle are the inputs of the empirical model. This model is available to the radiative transfer community as part of RTTOV. To investigate the variability of the FASTEM emissivity model, we selected 5 different ice surface categories among those available from Hewison and English (1999): 'First Year', 'Compact', 'Fast', 'Bare New', 'Bare New + Snow'. Fig. 1 summarises the spectral variation of the FASTEM ice emissivity across the 19-183 GHz range for all the 5 surface types: Fig. 1 a is for the SSMIS incidence angle (53.1°) and Fig. 1 b same as plot in a, but at nadir. The different surface types available in FASTEM were classified from aircraft observations and ground truth measurements of snow and ice thickness, density and water content taken in fixed sites. Figure 1 shows how the spectra of the ice emissivity varies with frequency and surface type as a consequence of the different mechanisms responsible for emission and scattering. For instance, the 'Bare New' category is characterised by a thick, homogeneous and flat ice unaffected by pressure ridging or snowfall. This surface presents a flat emissivity spectra. However, the presence of a thin layer of fresh, dry snow ('Bare New + Snow') introduces a slight dependency of frequency: lower frequencies have a higher effective emissivity as they penetrate the snow and consequently they sense the slightly warmer underlying surface. The 'Compact' and 'First Year' categories have a similar emissivity spectrum although different in magnitude: the lower emissivity at higher frequencies is characteristic of the volume-scattering mechanism of brine and air pockets
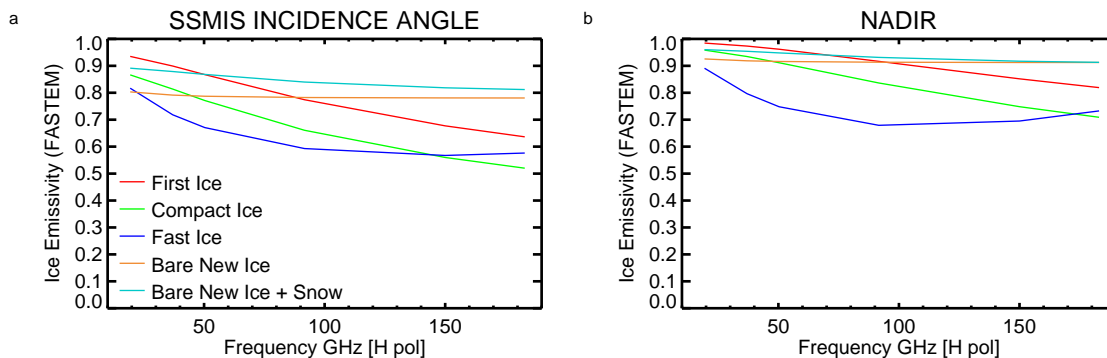
Figure 1: Models of ice emissivity (FASTEM) from different surface categories as in Hewison and English (1999): a, for SSMIS incidence angle (53.1°) and b, at nadir. Model values are for SSMIS frequencies (19.35, 37.0, 50.3, 91.65, 150.0 and 183.0 GHz) and are connected by a line to illustrate the trend.

within the icepack. These ice types, commonly referred to in the literature as multi-year and first-year ice, are generally very thick (ranging from 30 cm to 3 m) and they are also classified according to their age: first-year ice is defined as ice that has had no more than one winter growth, while multi-year ice has survived at least 2 melt seasons. The shift in emissivity value at the same frequency is basically due to different characteristics of the icepack: multi-year ice generally contains much less brine and more air pockets than first-year ice and consequently the intensity of the volume-scattering is larger reducing the emissivity as the frequency increases. However, the 'Fast' ice type is the category most affected by the volume-scattering mechanism and as a result the emissivity values below 100 GHz are additionally decreased.

4 Emissivity variability over ice from SSMIS observations

To evaluate the ice emissivity spectral signature from FASTEM we need additional independent estimates which can be considered as the 'true' measure of the surface emissivity. To do so we use the all-sky approach which can process SSMIS data and also retrieve the surface emissivity directly from satellite observations (Baordo et al., 2013; Baordo and Geer, 2015). In our study, we use the most recent version of the ECMWF assimilation system (cycle 41r2) in a configuration which allows only the monitoring of first-guess departures. This means that we run 'passive' experiments which do not take into account data assimilation and the atmospheric background is taken from a control. Basically, our reference is represented by a control experiment which uses emissivities retrieved from SSMIS channels (19.35, 37.0, 50.3, 91.65, 150.0 and also 183±7 GHz) to compute radiative transfer calculations. In addition, for every FASTEM ice model, we re-run the control experiment replacing the sea-ice emissivities derived from SSMIS observations with those calculated from Eq. 1 (a total of 5 experiments). The experiments were run at T1279 model resolution and for a total of 15 days (e.g. from 1 February 00UTC to 15 February 12 UTC) covering 4 different seasons: February 2015, May 2015, November 2014 and December 2014.

The overall sample of data from the 6 experiments matches the SSMIS observation space and it allows us to analyse the simulated emissivity spectrum and the magnitude of the first guess departures in every location where the IFS sea-ice fraction is greater than 0. However, to isolate the variability of the ice emissivity, in this section, we only consider those SSMIS retrievals which have been derived where the IFS C_{ice} is equal to 1. This is a very simple way to select those observations which are presumably
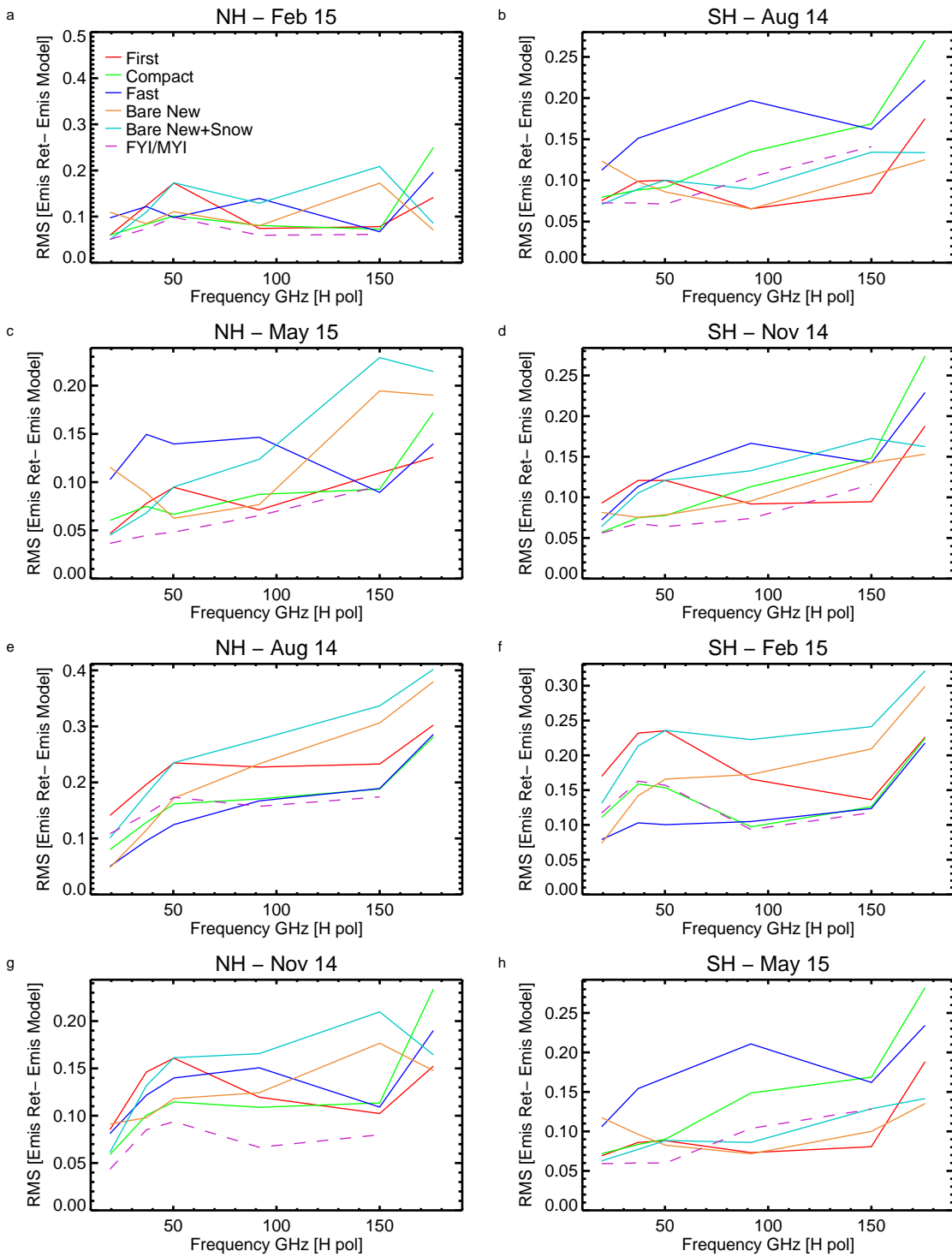
3

Figure 2: Root mean square of the difference between emissivities retrieved from SSMIS observations (where IFS C_{ice} is equal to 1) and the estimates from FASTEM models (1 coloured line for every FASTEM ice type) as a function of SSMIS windows channels (19.35, 37.0, 50.3, 91.65, 150.0 and 183±7 GHz). Plots are grouped according to the same season in the Northern and Southern hemisphere: winter (a and b), spring (c and d), summer (e and f) and autumn (g and h). Purple dashed line indicates the experiment which discriminates between the use of the FASTEM 'First' or 'Compact' ice emissivity.

not contaminated by the presence of open water. Figure 2 explores the ice emissivity variability in terms of root mean square (RMS) of the difference between the SSMIS retrievals and the estimates from the FASTEM model as a function of frequency. RMS is separately computed for the Northern and Southern hemisphere and for every season (winter, spring, autumn, summer). Results encapsulated in Fig. 2 clearly highlight the difficulty of modelling the ice emissivity across the 19-183 GHz range: for instance, in the Southern hemisphere during summer (Fig. 2 f), the 'Fast' ice type seems to be the best choice to minimise the RMS, but in winter (Fig. 2 b) this model is the worst by up to 10% across the frequencies. The possibility of classifying different ice types from the satellite measurements might help in reducing the uncertainty on the emissivity. We found a criteria to identify first-year ice (FYI) or multi-year ice (MYI) from SSMIS observations and it will be discussed in Sect. 5. However, in Fig. 2 we also examine the beneficial impact of using this methodology. The dashed purple line indicates the results for the experiment which implements the clustering of the ice surface from SSMIS measurements. In the Northern hemisphere is clear that the discrimination of ice types provides the smallest RMS across all the frequencies. In the South Pole, results are mixed although the classification might still help in some cases. For the dashed purple line we omitted the RMS value at 183 GHz: the FASTEM emissivity models computed at 183 GHz systematically diverges from the estimate provided by the SSMIS observations at 183±7 GHz. This behaviour suggests a deficiency in the parametric models for frequencies above 150 GHZ. We will mainly focus on this problem in the rest of the report.

To better compare the emissivity spectrum obtained from SSMIS observations with that from the parametric ice models, Fig. 3 shows mean and standard deviation of retrieved emissivities as a function of frequency. Statistics are computed considering the same sample of data which has been used to calculate the RMS in Fig. 2. Figure 3 provides a clearer picture of the possibility to identify a particular FASTEM model which can reasonably fit the observations. During summer, the shape of the SSMIS emissivity spectrum appears to be well approximated by the 'Fast' ice category, but for the other three seasons results are mixed. At lower frequencies (19, 37 and 50 GHz) the 'Compact' ice might be a reasonable choice to model emissivity in both the hemispheres, whilst at higher frequencies (91 and 150 GHz) the 'First Year' category might be preferable although for the Northern hemisphere statistics suggest that it might be important to cluster the two surface types. Figure 3 also demonstrates that the emissivity observed at 183±7 GHz (with the exception of the summer case, plots e and f) is consistently higher than the estimates provided by the 'Compact', 'First Year' and 'Fast' models at 150 and 183 GHz. Such behaviour is in agreement with the observed emissivity spectrum which has been previously measured from Hewison et al. 2002 (and also Hewison 2002) in the context of the POLEX-SEPOR (Polar Experiment - Surface Emissivity in Polar Regions) campaign conducted by the Met Office in March 2001. Microwave radiometers, also equipped with 183 GHz channels, were operated on a research aircraft in order to estimate the emissivity of various arctic surfaces. The measurements showed that the emissivity of older ice types decreases as the frequency increases, but usually starts to increase from 157 to 183 GHz.

We can conclude that the signal we are retrieving from satellite observations for winter, spring and autumn is most likely a real characteristic of the surface emissivity at higher microwave frequencies. However, we wonder why we are not observing a similar feature during summer. To assess the reliability of the retrievals we simply analyse the values of the surface to space transmittance, which can provide an indication of the sensitivity to the surface for a particular frequency, and the number of successful retrievals (value of emissivity between 0 and 1). We briefly address this issue considering the winter and summer cases in the Northern hemisphere, but the same conclusions can be drawn for the equivalent seasons in the Southern hemisphere. Figure 4 shows the mean model transmittance and the number of successful retrievals corresponding to the sample of data as in Fig. 3 a (Northern hemisphere, winter) and Fig. 3 e (Northern hemisphere, summer). The amount of atmospheric water vapour in polar regions tends to be very low because of the low temperatures. This means that the atmosphere can be very dry during winter allowing a good visibility of the surface also at higher microwave frequencies. On the contrary, during summer, the concentration of water vapour is larger, the atmosphere can be optically
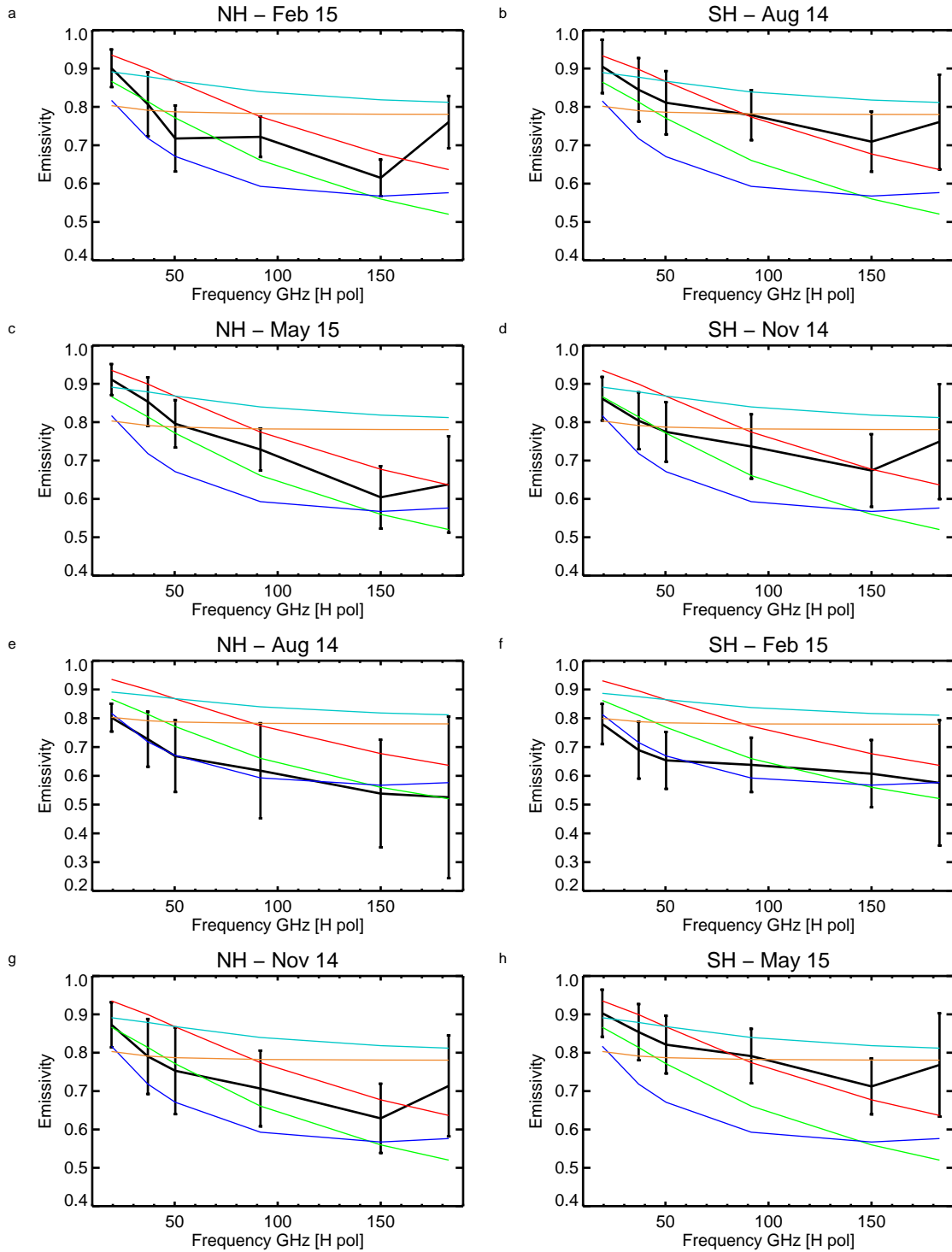
Figure 3: Mean and standard deviation (error bars) of ice emissivity retrieved from SSMIS channels (19.35, 37.0, 50.3, 91.65, 150.0 and 183±7 GHz). Statistics are computed considering the same sample of data as in Fig. 2. As a reference, coloured lines indicate the emissivity spectrum from the FASTEM ice models as in Fig. 1 a.
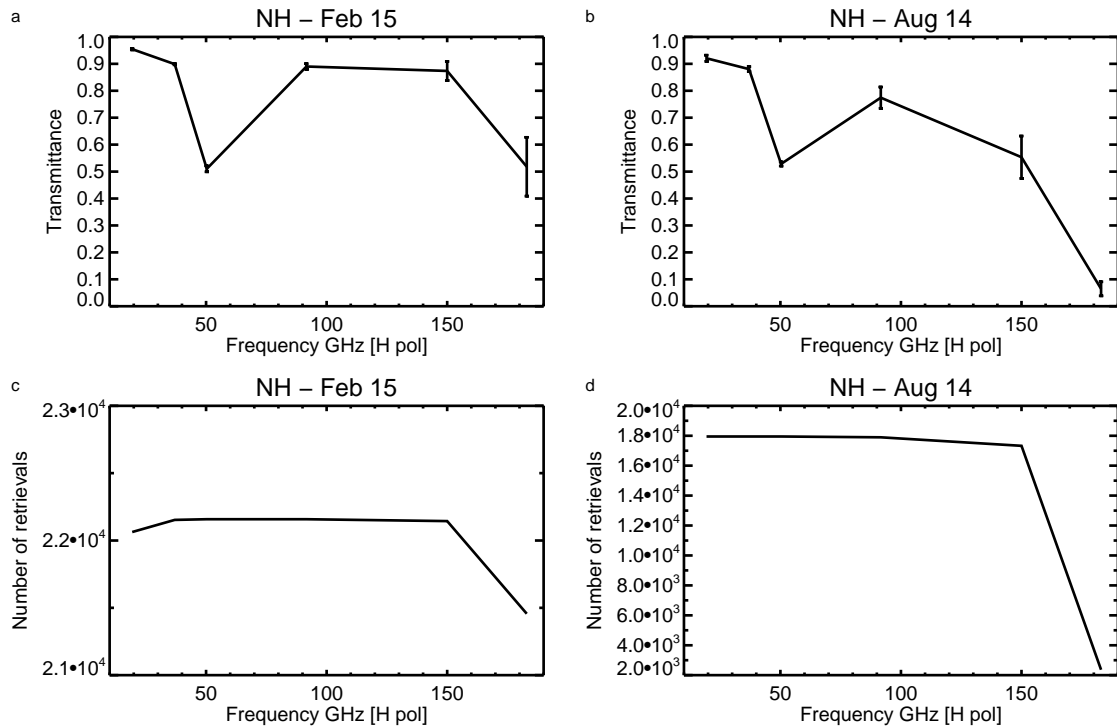
Figure 4: Mean and standard deviation (error bars) of model transmittance (a and b) and number of successful retrievals (c and d) corresponding to equivalent sample of data as in Fig. 3 a and e.

thicker and consequently the retrieval above 50 GHz can be increasingly affected by errors. We need to take into account that our retrievals might additionally be affected by cloud contamination as the calculation is embedded within the all-sky path of the ECMWF system which considers clear, cloudy and precipitating scenes. Figure 4 shows that during winter, the transmittance has on average large values across the 19-183 GHz range and this allows a good sensitivity to the surface. As a consequence the number of successful retrievals is stable across all the frequencies with a 2% failure rate at 183 ± 7 GHz. The stability of the retrievals at 183 ± 7 GHz is also confirmed by the small standard deviation as showed in Fig. 3 a. In summer, the higher frequencies present on average smaller values of transmittance due to the increase in water vapour and/or cloud contamination. This mainly affects the performance of the retrieval at 183 ± 7 GHz which most likely is noisy: the sample of retrieved emissivity is small (about 80% of failures) and it is characterised by a large standard deviation as showed in Fig. 3 e.

5 Clustering surface ice type

Discriminating the ice surface type in order to use the best FASTEM ice emissivity model might result in a better modelling of emissivity over sea-ice. However, we do not have a parameter within IFS which classifies different ice categories. To cluster the surface types we investigated the possibility to use SSMIS observations. To guide our analysis we used the sea-ice products provided by the Ocean and Sea Ice Satellite Application Facility (OSI SAF) (Breivik et al., 2001). Sea-ice fields such as ice concentration and ice type, which are derived from SSMIS and ASCAT data, are produced daily for the Northern and the Southern hemisphere in a 10 km resolution grid. The OSI ice type is divided in two classes: first-year and multi-year ice, where multi-year means ice that has survived at least one summer season. Due to the high resolution of the grid, we averaged the OSI products in boxes of approximately
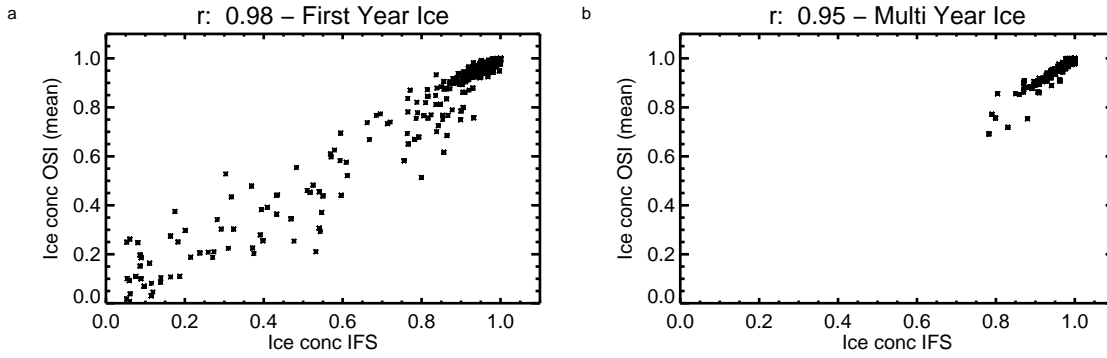
Figure 5: Relationship between the sea-ice concentration from IFS and the averaged value from the OSI estimates. The sample of data, which refers to the SSMIS/IFS space for the 1 February 2015 in the Northern hemisphere, is also divided according to the OSI ice type: a, first-year and b, multi-year. Plots also show the Pearson correlation coefficient (r).
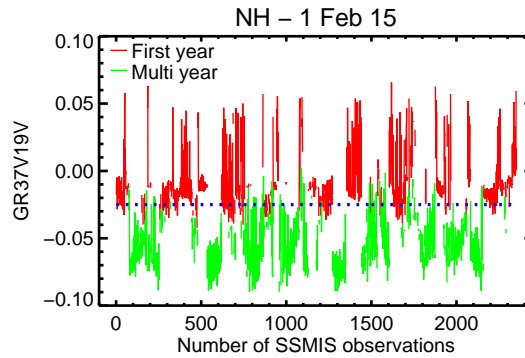

Figure 6: Observed GR37V19V in the Northern hemisphere classified according to the OSI first-year of multi-year ice. Blue dashed line indicates constant value of -0.025. SSMIS observations are for the 1 February 2015 from 9 to 21 UTC.

60 km by 60 km in order to roughly match the magnitude of the 'superobbing' applied to the SSMIS observations in the all-sky framework (Geer and Bauer 2010). In our approach, the final ice type (first-year or multi-year) in the equivalent SSMIS/IFS grid point is simply the OSI ice type which has the larger number of counts. In the case of an equal number of occurrences we arbitrarily classify the pixel as first-year ice. Figure 5 is an example of the relationship between the sea-ice concentration from IFS and the averaged value from the OSI estimates. The sample of data, which is also split into the two ice categories, is highly correlated. To explore the possibility of identifying first-year and multi-year ice from SSMIS data, we mapped the OSI ice type over the SSMIS observation space. We found that the SSMIS gradient ratio (GR) given by:

$$GR37V19V = \frac{T_b(37V) - T_b(19V)}{T_b(37V) + T_b(19V)}, \qquad (2)$$

can be reasonably used as a predictor to reproduce the discrimination of ice types provided by the OSI product. This is demonstrated by Fig. 6 which shows the observed GR37V19V in the Northern hemisphere categorised according to the OSI ice type. The use of a constant threshold of -0.025 seems to be good enough to grossly classify the ice category: we consider first-year ice where the SSMIS GR is
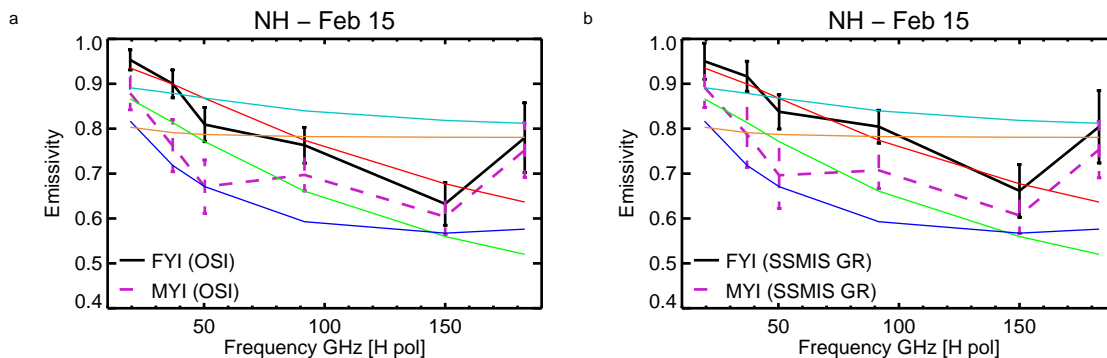
Figure 7: Mean and standard deviation of retrieved emissivities as a function of frequency as Fig. 3 a, but splitting the retrievals taking into account the classification of first-year ice (FYI) and multi-year ice (MYI) from the OSI product (a) and the observed SSMIS GR (b).

greater than -0.025, multi-year ice otherwise. To verify this gross check criteria, we re-plot the mean and standard deviation of retrieved emissivities as a function of frequency, but splitting the retrievals taking into account the surface categorisation respectively from the OSI product and the observed SSMIS GR. Figure 7 shows the results of this approach for the wintertime in the Northern hemisphere. The effect of clustering the surface type gives a positive outcome independently of the OSI or the SSMIS GR classification. The two sample of retrievals identify two distinct spectral signatures of the surface: the multi-year ice, associated with lower emissivity values and the first-year ice, characterised by larger values across all the frequency range. The emissivity spectrum (below 150 GHz) of the FASTEM 'First' ice category seems to fit really well that generated by the retrievals classified as first-year ice. The FASTEM 'Compact' emissivity model, instead, reasonably fits the observations classified as multi-year ice at higher microwave frequencies (91 and 150 GHz), whilst at lower frequencies (37 and 50 GHz) the observed emissivity spectrum appears to be closer to that generated by the FASTEM 'Fast' ice type.

6 Impact on SSMIS first-guess departures

We now investigate the impact of using different estimates of sea-ice emissivity on the calculation of the simulated brightness temperatures. This is done through Fig. 8 which shows histogram of first-guess departures for 6 different SSMIS channels. For each frequency, we explore the departures computed from our 6 experiments and this gives an indication of which surface emissivity is doing a better job in simulating the observations. The number of successful SSMIS retrievals at each frequency coupled with the locations where the IFS C_{ice} is greater than 0 define the sample of our data over sea-ice. To simplify our analysis, in Fig. 8, we only show the distribution of first-guess departures for the winter season in the Northern hemisphere, but results can be generalised to the other seasons and the Southern hemisphere. It is worth pointing out that in the calculation of the first-guess departures obtained from the FASTEM emissivity models (Eq. 1) we use the FASTEM estimate at the SSMIS channel, except for the humidity sounding channels where we simply take the FASTEM estimate at 183 GHz. In the case of the emissivity retrieved from SSMIS observations, we reassign the retrieved emissivity to the closest channel higher in frequency (taking care to use the right polarisation) in order to perform radiative transfer calculations. By construction, the simulations would be identical to the observations if we used the emissivity retrieved for the same channel. The criteria to reassign emissivities is as follows: 19 GHz retrievals are applied to 37 GHz; 37 GHz to 50 and 91 GHz; 50 GHz to temperature sounding channels; 91 GHz to 150 GHz; 150 GHz to humidity sounding channels. Of course, at 19 GHz, there is no possibility to assign an estimate of emissivity coming from a lower frequency. As expected, due to

the high variability of ice emissivity in frequency, the use of emissivity retrieved at 19, 37 and 91 GHz to simulate radiances at 37, 91 and 150 GHz is badly wrong (Fig. 8 a, c and d). At 37 GHz, parametric models to emulate emissivity over sea-ice do not bring large improvements either. At 91 and 150 GHz, the parametric models gives slightly better results than the retrievals. The use of the FASTEM 'First' ice type, compared to the retrievals, moves the departures in the right direction producing a more symmetric distribution of first-guess departures although the values are still large. Results for the sounding channels are more promising. The magnitude of first-guess departures for the temperature sounding channel at 52.8 GHz is generally small. The distribution of the departures seems also be characterised by a reasonable symmetry. It looks also quite plausible to model the emissivity through the use of FASTEM. In agreement with Fig. 3 a, we might identify the 'Compact' ice type as the category which might be globally used to simulate the ice emissivity around the 50-55 GHz range. The purple dashed line in a, b, c and d explores also the impact of discriminating the use of the FASTEM 'First' or 'Compact' ice emissivity according to SSMIS observations. The surface clustering provides a clear benefit between the 50-150 GHz range.

At 183 GHz, departures for the humidity sounding channels confirm that the FASTEM model is providing a wrong estimate of emissivity. The tail of positive first guess departures indicates that the observations are systematically warmer than the simulated radiances and this implies that the emissivity used in the calculations is too low. This is also demonstrated by two facts: 1) experiments which uses a larger emissivity value ('Bare New' and 'Bare New + Snow') are able to move the distribution of departures in the correct direction. 2) Emissivity retrieved at 150 GHz and assigned to the humidity sounding channels is doing a better job than the emissivity model, but, at 183 ± 7 GHz, which is the channel most sensitive to the surface, the distribution is still clearly shifted too far to the right. This indicates that the real emissivity around 183 GHz must be larger than that estimated at 150 GHz in agreement with the results of Fig. 3. With the limited time period available for the visiting scientist mission, we decided to mainly focus our job on the possibility to find a criteria to improve the estimate of the ice emissivity at 183 GHz which might be beneficial to the assimilation of satellite observations over sea-ice.

7 Modelling ice emissivity for 183 GHz channels

Results of Fig. 3 indicate that the emissivity at 183 GHz is consistently higher than that at 150 GHz in every time of the year and polar region. We wonder if it is reasonable to create a simple model which might linearly increase the emissivity estimate at 150 GHz. Relying on the SSMIS emissivity retrievals we searched for a linear regression which satisfies the relation:

$$\varepsilon_{183} = m\varepsilon_{150} + q. \tag{3}$$

To estimate m and q we used the sample of retrievals in winter, autumn and spring with the following conditions verified simultaneously:

a) $0 < \varepsilon_{183} < 1$,
b) $0 < \varepsilon_{150} < 1$,
c) IFS $C_{ice} = 1$,
d) $\tau_{183} > 0.4$.

Basically a, b and c, as previously done (e.g. Fig. 3), are for looking at successful retrievals most likely not contaminated by open water and d, which uses the transmittance at 183 ± 7 provided by the model, can preserve a good visibility of the surface rejecting those observations which are presumably affected by water vapour and/or cloudy conditions.
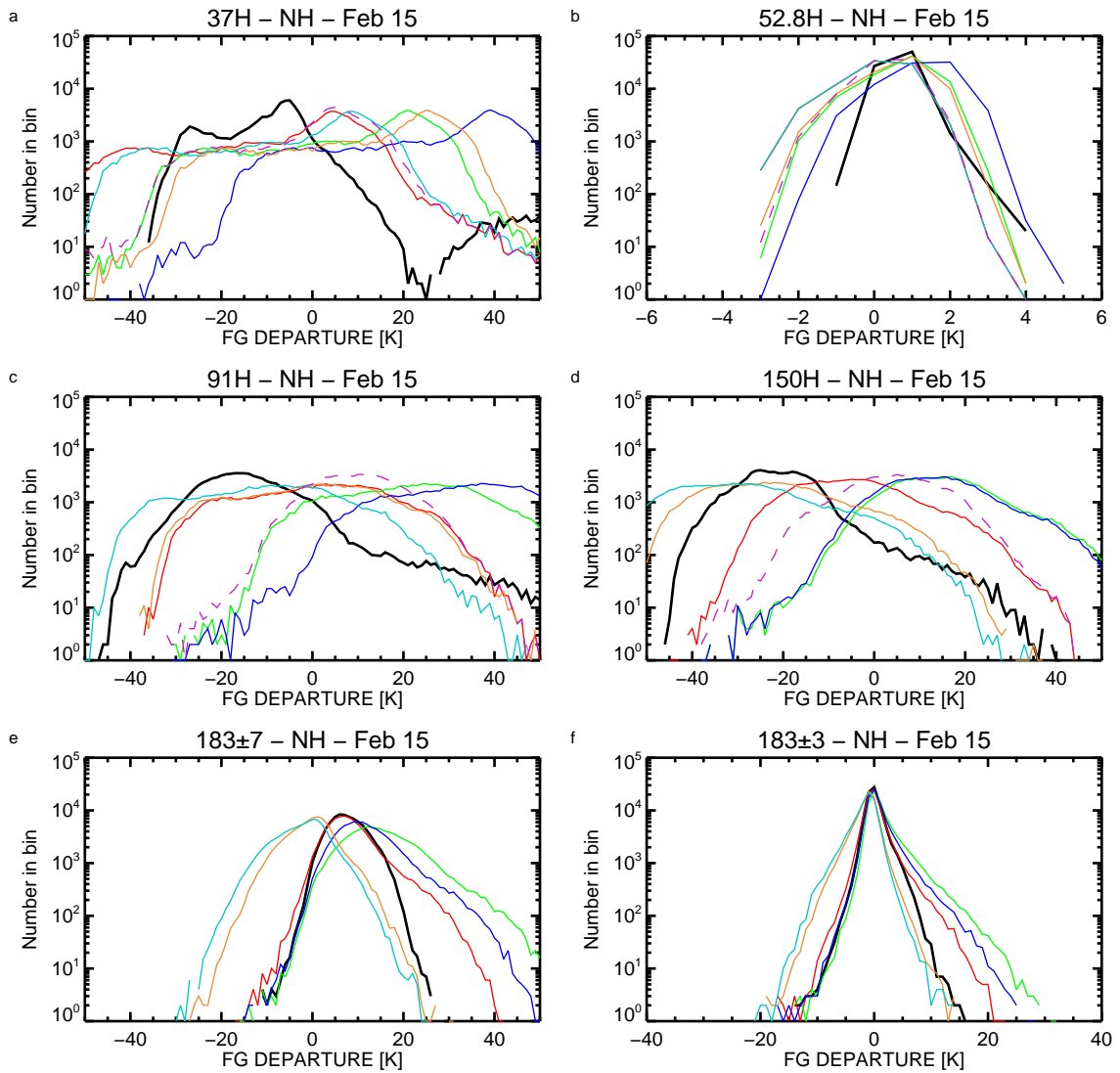
Figure 8: Histogram of first-guess departures for 6 different SSMIS channels. Data are referred to the winter season in the Northern hemisphere, taking into account every successful SSMIS retrieval where IFS C_{ice} is greater than 0. The black line is for simulated radiances computed using the emissivity retrievals, whilst coloured lines indicate the use of the emissivity derived from Eq. 1 for every FASTEM ice model. Purple dashed line indicates the experiment which discriminates between the use of the FASTEM 'First' or 'Compact' ice emissivity.
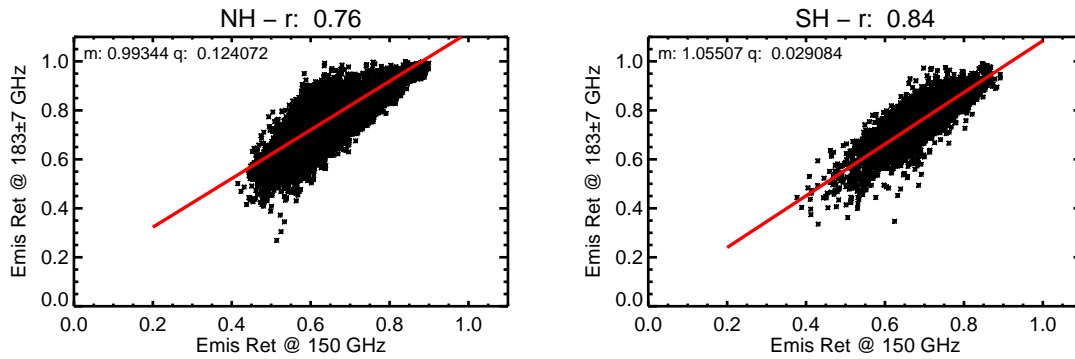
Figure 9: Relationship between retrieved emissivity at 183±7 and 150 GHz obtained from observations in winter, spring and autumn in the Northern (NH) and the Southern (SH) hemisphere. Retrievals are selected considering locations where model values of sea-ice concentration and transmittance at 183±7 are respectively equal to 1 and greater than 0.4. Plots also show the Pearson correlation coefficient (r) and the coefficients (m and q) from the linear regression.

The relationship between the retrievals at 183±7 and 150 GHz is examined through Fig. 9 and Fig. 10 which summarise the results of the linear regression providing the values for the coefficients m and q. The Pearson correlation coefficient is also shown. The relation is separately evaluated for the Northern and Southern hemisphere: Fig. 9 considers retrievals from observations in winter, spring and autumn, whilst Fig. 10 analyses the sample of data for different seasons. Figure 9 and 10 are completed by Table 1 which, for every set of coefficients, shows the values of the ice emissivity at 183 GHz computed from the linear approximation applied to the FASTEM 'First' and 'Compact' emissivities at 150 GHz.

The relationship between the retrievals at 183±7 and 150 GHz appears to have a seasonal and geographical dependency and consequently the emissivity at 183 GHz computed from 'boosting' the FASTEM emissivity at 150 GHz varies with the estimated set of coefficients. For instance, considering the winter season, the linear approximation applied to the FASTEM 'First' ice category generates the largest change in the emissivity (28%) in the North Pole and the lowest (14%) in the South Pole. It is questionable whether the Northern and the Southern hemisphere present such different characteristics in the ice surface emissivity which might justify the results of the linear interpolation. Due to the limited time available, we globally tested the emissivity linear model using the coefficients m and q derived considering retrievals from all the three seasons (Fig. 9). To do so we run 2 additional experiments which compute the emissivity for the humidity sounding channels through Eq. 5. The first experiment (named as 'FYI boosted') uses the ice emissivity provided by the FASTEM 'First' ice category, whilst the second (named as 'Retr boosted') uses retrieved emissivities from SSMIS observations. Considering that the use of the observed SSMIS GR is very easy to implement within IFS, we also decided to run another experiment to evaluate the impact of clustering the surface type on the simulated brightness temperatures. In this experiment (named as 'FYI/MYI boosted') we firstly classify the surface type as first-year or multi-year ice and, secondly, according to the surface which has been identified, we linearly boost the FASTEM 'First' or 'Compact' emissivity at 150 GHz. Results are analysed in next section.

8   Using the linear model to calculate emissivity at 183 GHz

In this section we present the results of using the linear model to boost the emissivity at 150 GHz in order to have an estimate for the 183 GHz channels. Table 2 provides the summary of the 5 experiments which have been used to globally evaluate the emissivity linear model. It is worth mentioning that in
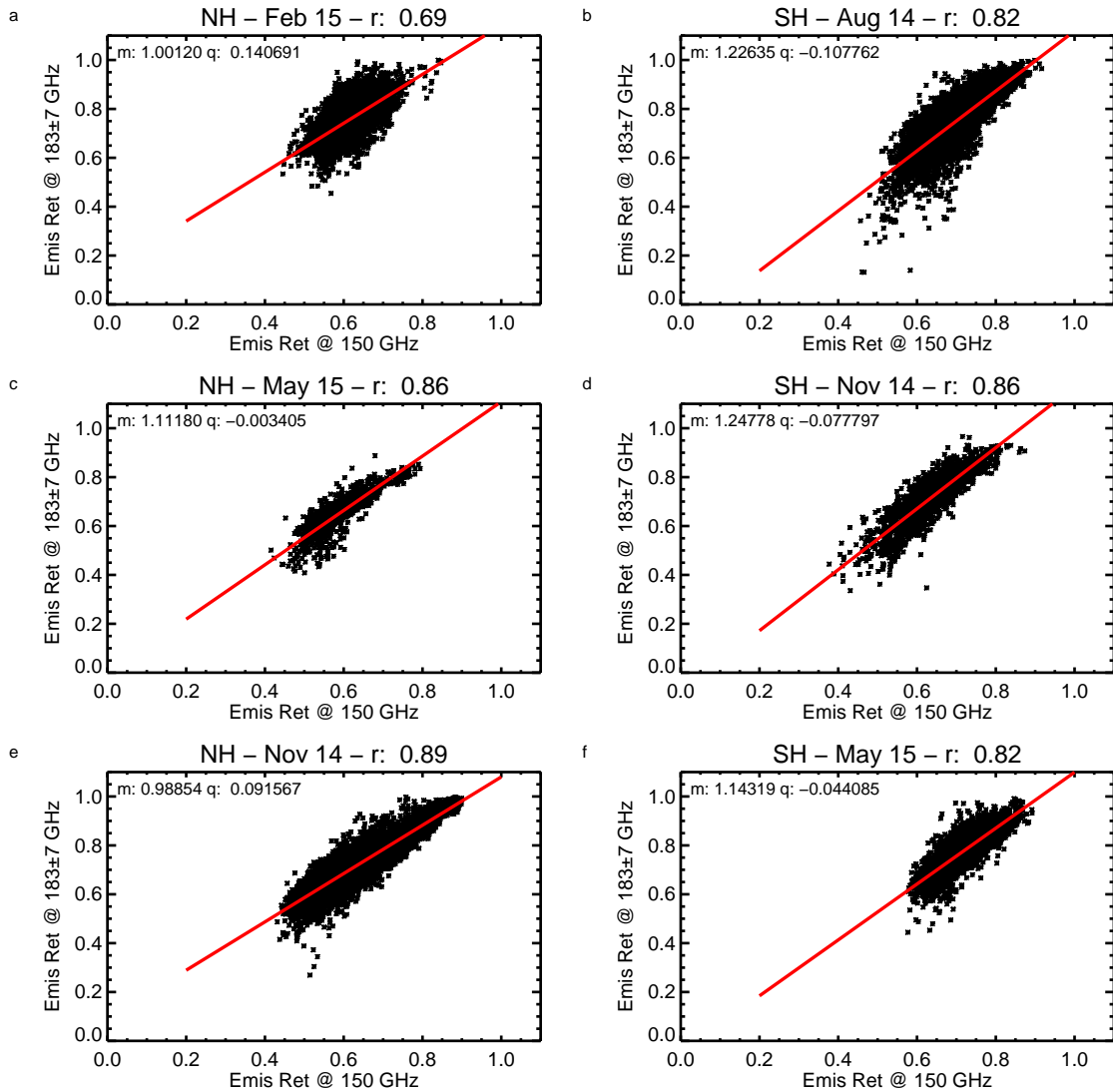
Figure 10: As Fig. 9, but splitting the sample of data according to the season: winter (a and b), spring (c and d) and autumn (g and h).

Table 1: FASTEM emissivities at 150 and 183 GHz (for SSMIS incidence angle and polarisation) for the 'First' and 'Compact' ice categories compared to the equivalent estimates at 183 GHz computed through the linear approximation. Emissivities for the Northern (NH) and the Southern (SH) hemisphere are calculated from Eq. 5 using coefficients m and q shown in Fig. 9 and Fig. 10. Percentages indicate the change respect to the FASTEM ice emissivity at 183 GHz (FASTEM-'First' or FASTEM-'Compact').

	ε_{150}	ε_{183}
FASTEM-'First'	0.677278	0.636455
FASTEM-'Compact'	0.559852	0.520112
ε_{183} from ε_{150} FASTEM-'First'	NH	SH
All seasons	0.796907 (25%)	0.743660 (17%)
Winter	0.818782 (28%)	0.722818 (14%)
Spring	0.749593 (18%)	0.767297 (21%)
Autumn	0.761083 (20%)	0.730172 (15%)
ε_{183} from ε_{150} FASTEM-'Compact'	NH	SH
All seasons	0.680251 (31%)	0.619767 (19%)
Winter	0.701215 (35%)	0.578812 (11%)
Spring	0.619038 (19%)	0.620775 (19%)
Autumn	0.645003 (24%)	0.595932 (14%)

Table 2: Summary of experiments to globally evaluate the linear model to estimate emissivity at 183 GHz.

Experiment Name	ε_{183}	Linear Boost	Line (Plot)
Retr	Retrieved @ 150 GHz	No	Black
FYI	FASTEM 'First' @ 183 GHz	No	Red
FYI boosted	FASTEM 'First' @ 150 GHz	Yes	Dashed blue
FYI/MYI boosted	FASTEM 'First'/'Compact' @ 150 GHz	Yes	Dashed green
Retr boosted	Retrieved @ 150 GHz	Yes	Dashed black

the experiment that boosts the SSMIS emissivity retrieved at 150 GHz, we apply the linear model only for those observations where the IFS C_{ice} is greater than 0.5, while for smaller values of ice-fraction we use the FASTEM emissivity over ocean. We would hope to improve this aspect in future. The outcome of the experiments, for every season and polar region, is examined through 4 figures: Fig. 11 and Fig. 12 show histograms of first-guess departures respectively for 183±7 and 183±3 GHz; Fig. 13 and Fig. 14 provide a more general statistical summary showing standard deviation and skewness of first-guess departures for the 183 GHz channels.

Histograms of first-guess departures visibly provide two main results: 1) the linear model is always able to correct the positive tail of first guess departures which characterises the 'FYI' experiment. Hence, the too low FASTEM emissivity at 183 GHz is correctly adjusted. 2) Clustering the ice surface type seems to make a positive difference only for the Northern hemisphere, while the single ice classification as first-year appears to be sufficient for the South Pole. However, the magnitude of the improvements from the linear approximation can be better quantified through Fig. 13 and Fig. 14. We search for the scenario where, comparing with the results from the 'FYI' or 'Retr' experiment, the equivalent boosted experiment presents a reduction (or similar size) in the standard deviation and a skewness which tends to zero. The winter and autumn cases are those which are characterised by the best results. For the North Pole the discrimination between first-year and multi-year ice from the observed SSMIS GR clearly provides an additional improvement in respect to the case in which we classified the ice type only as first-year. This is not the case for the Southern hemisphere where the categorisation of the the ice surface as first-year appears to be the best choice. Results for the summer case are neutral for the Northern

hemisphere and slightly in favour of the 'FYI boosted' experiment in the Southern hemisphere. The small size and the quite good symmetry of the first guess departures suggest that at this time of the year the atmosphere is most likely optically thicker and consequently the radiative transfer calculations are not strongly influenced by the surface emissivity. For the springtime, we still observe improvements for the South Pole, but slight degradation for the North Pole. This result suggests that it might be relevant to use a different set of coefficients to diversify the linear model across the seasons. For the spring case, we are using a set of coefficients which are probably boosting too much the emissivity as also demonstrated by the departures at 183±7 GHz (Fig. 11 c). Instead, the use of the coefficients derived for this season (as in Table 1) would have provided a smaller estimate of emissivity and a better fit to observations.

Maps of mean first guess departures are also helpful in evaluating the use of the boosted emissivity: Figure 15 and 16 show mean first guess departures respectively for the North and South Pole during the winter period, while Figure 17 and 18 are the equivalent for autumn. Figures analyse the results of the linear model comparing the departures at 183±7 and 183±3 GHz obtained from the retrieved emissivities at 150 GHz ('Retr' experiment) with those computed from the 'Retr boosted' experiment. The general outcome is that the large positive departures at 183±7 which characterised the 'Retr' experiment are always removed. Positive biases appear to remain in those regions where the IFS C_{ice} is less than 0.5 where the 'Retr boosted' uses the open water emissivity from FASTEM. Positive first guess departures also are decreased at 183±3. However, results suggest that tuning the linear model is very important otherwise, boosting too much the surface emissivity, we might generate a sample characterised this time by negative biases.

Another way to study the reliability of the linear boost approximation is to observe the variability of the emissivity and first-guess departures in the same geographical location (e.g. time series of data). To do so we selected a point in the Barents Sea (76.84°N; 47.81°E) which was observed by 53 SSMIS overpasses for the period ranging from 1 to 15 February 2015. Figure 19 provides a summary of this case study. The observed SSMIS GR classifies the ice type along this cross section as first-year in agreement with the OSI product. This means that results of the 'FYI boosted' and 'FYI/MYI boosted' experiments are identical and consequently plots in Figure 19 show only the green dashed line associated with the 'FYI/MYI boosted' experiment. This geographical location has been also chosen because it is characterised by values of IFS C_{ice} always smaller than 1 and this allows to evaluate the computation of the emissivity over-sea ice from Eq. 1 as the weighted average of the ocean and ice emissivity. Figure 19 a compares the variability of the IFS sea-ice concentration with that from the OSI (mean and standard deviation). The two quantities have a very good match apart from a set of measurements which have different behaviour. For about 24 hours the IFS predicts an high sea-ice concentration (0.76) whilst the equivalent OSI estimate is almost zero (0.07). This actually happens from the 5 February 3.32 UTC (overpass 24) to the 6 February 13.22 UTC (overpass 34) when the IFS sea-ice fraction drops to 0.07. This behaviour is not particularly surprising: the IFS sea-ice concentration is from the Operational Sea Surface Temperature and Sea Ice Analysis (OSTIA, Donlon et al., 2011) and for processing reasons is about 24 hours delayed in respect to the OSI product. However, it is questionable whether it is better to rely on a product which might have a more accurate processing even though it might be less efficient in capturing daily changes in the sea-ice surface. As a reference, Figure 19 a also shows the SSMIS emissivity retrieved at 19H. It is very interesting how the emissivity is highly correlated to the sea-ice fraction and how the change that happened on the 5 February is well captured. This is an indication that it might be possible to retrieve the sea-ice concentration exploiting the surface emissivity at 19 GHz. The possibility of retrieving the sea-ice concentration from SSMIS emissivity retrievals is briefly discussed in the Appendix. Figure 19 b provides the variability of the model transmittance across the 19-183 GHz range. Transmittance at 150 GHz is always larger than 0.8 and it confirms the feasibility of retrieving the emissivity because of a very high surface sensitivity. Also the visibility of the surface at 183±7 GHz seems to be reasonably good. However, when the transmittance becomes too low (less than 0.4) we might have an incorrect estimate (probably too large) or a failure in the retrieval (e.g. overpass 34 in 19 c). The effect of boosting the emissivity is explored in Figure 19 c and d. For every overpass where the
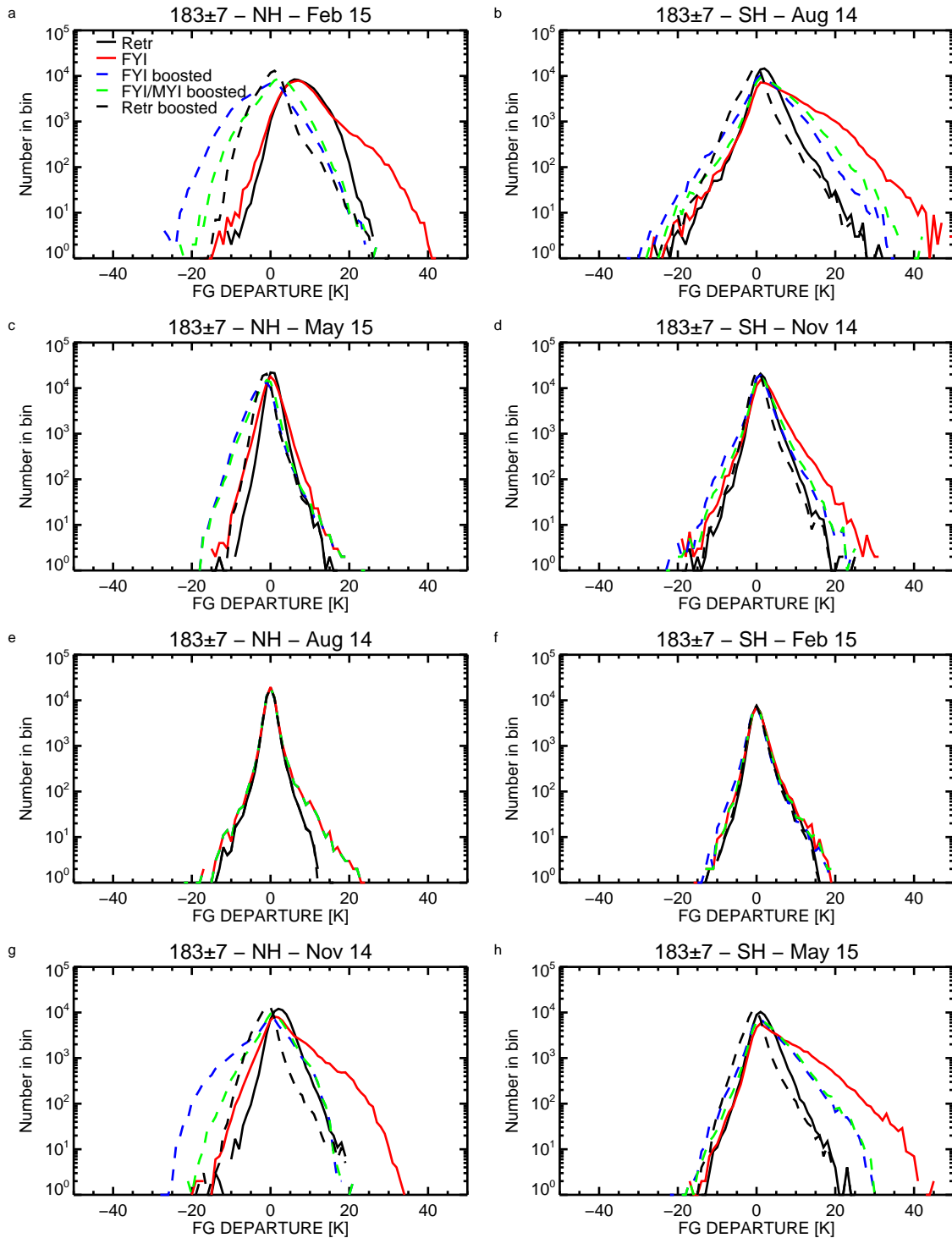
Figure 11: Histograms of first-guess departures for SSMIS 183±7 GHz channel. Data takes into account every successful SSMIS retrieval where IFS C_{ice} is greater than 0. Plots are grouped according to the same season in the Northern and Southern hemisphere: winter (a and b), spring (c and d), summer (e and f) and autumn (g and h). Different coloured lines are for different experiments as summarised in Table 2.
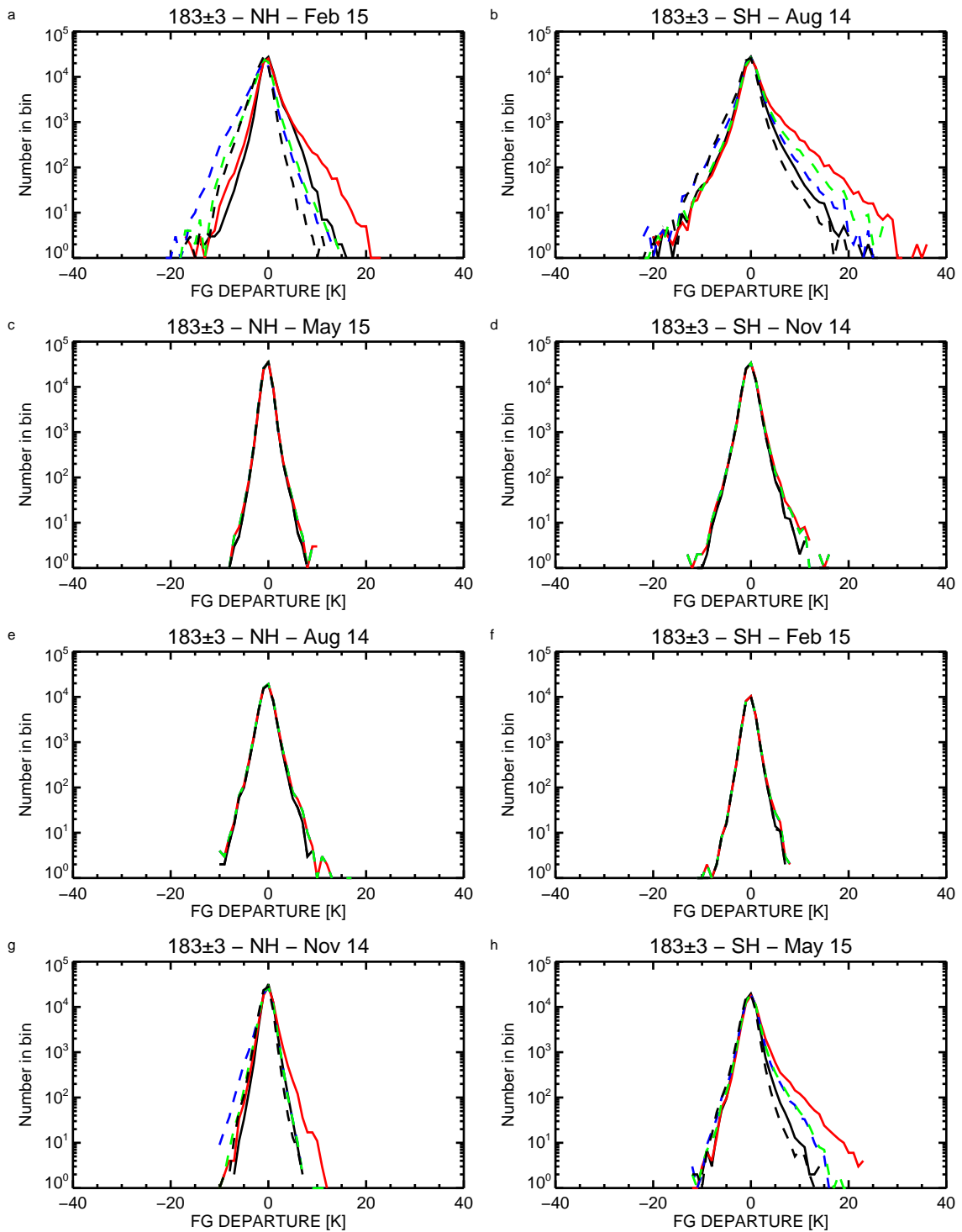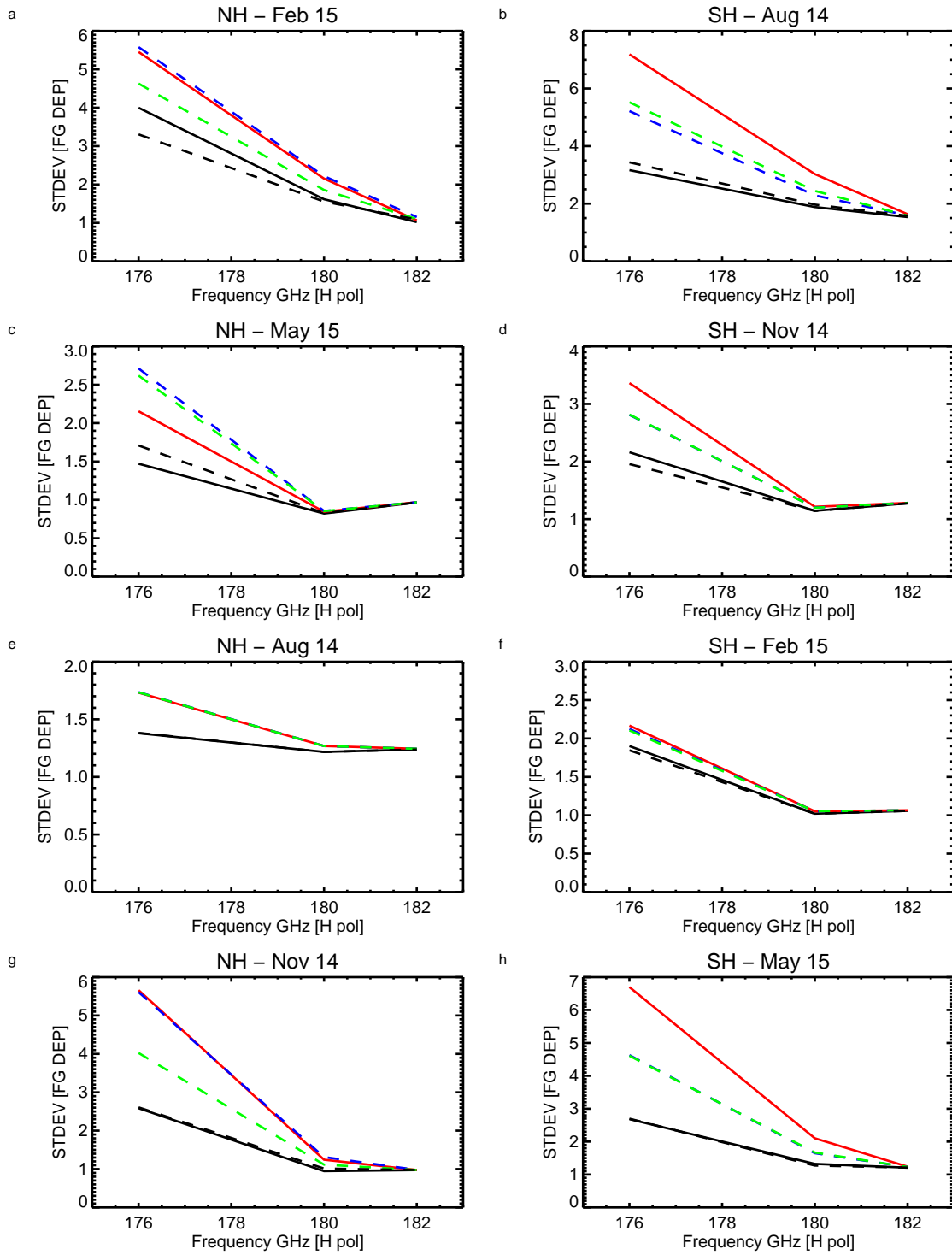
Figure 12: As Fig. 11, but for SSMIS 183±3 GHz channel.

Figure 13: As Fig. 11, but showing standard deviation of first-guess departures for SSMIS humidity sounding channels. Channels at 183±7, 183±3 and 183±1 are respectively associated with frequencies at 176, 180 and 182 GHz.
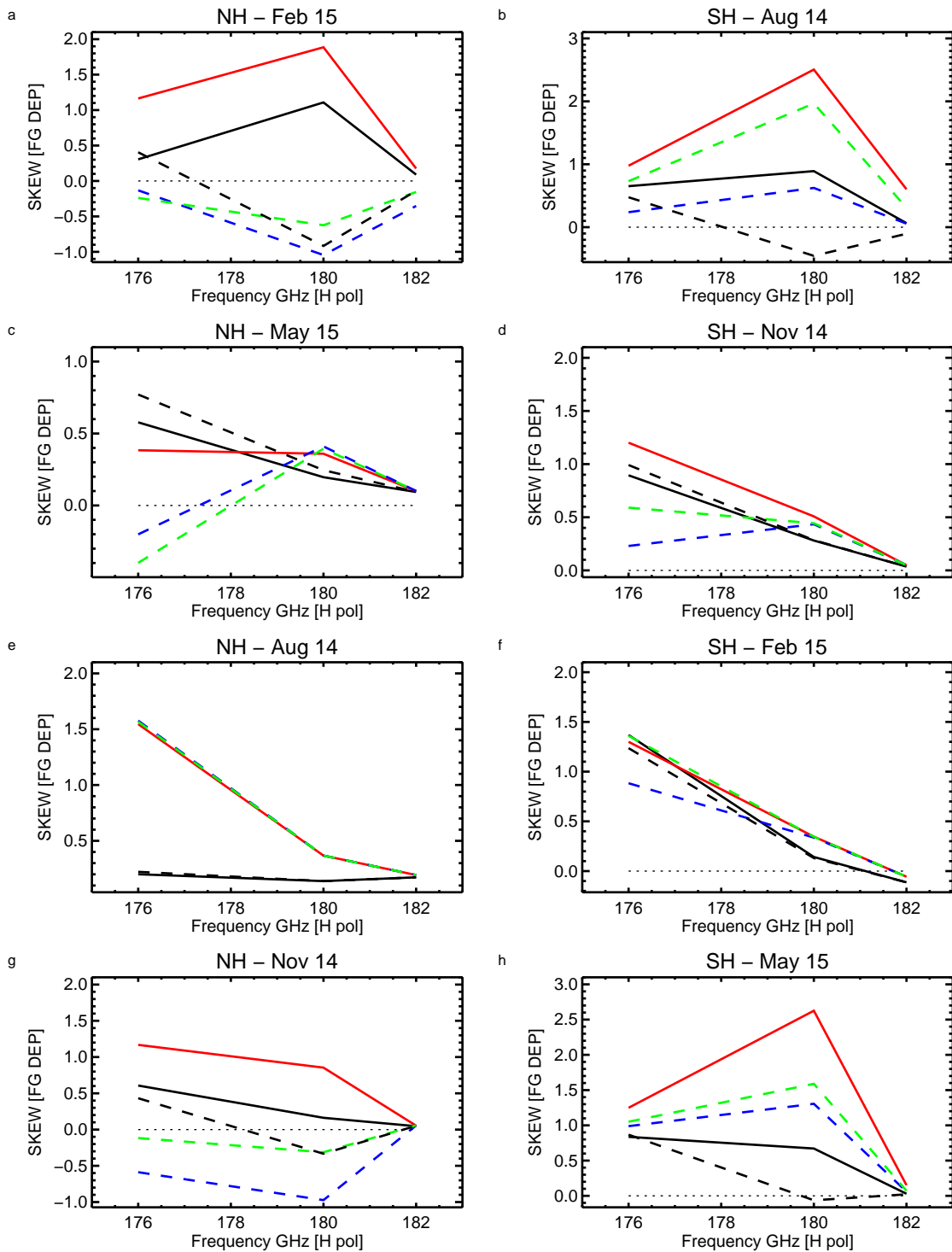
Figure 14: As Fig. 13, but showing skewness of first-guess departures.
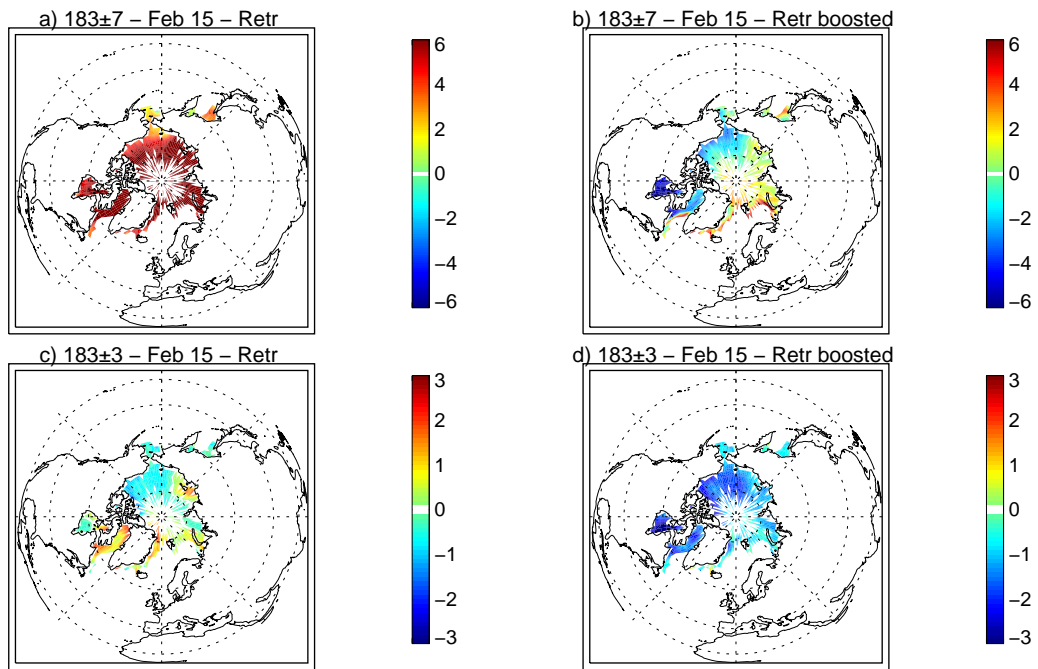
Figure 15: Mean maps of first guess departures for SSMIS humidity sounding channels (183±7 and 183±3 GHz) from 1 to 15 February 2015. Simulations from retrieved emissivities at 150 GHz (a and c) are compared to those provided by the 'linear boost model' (b and d).
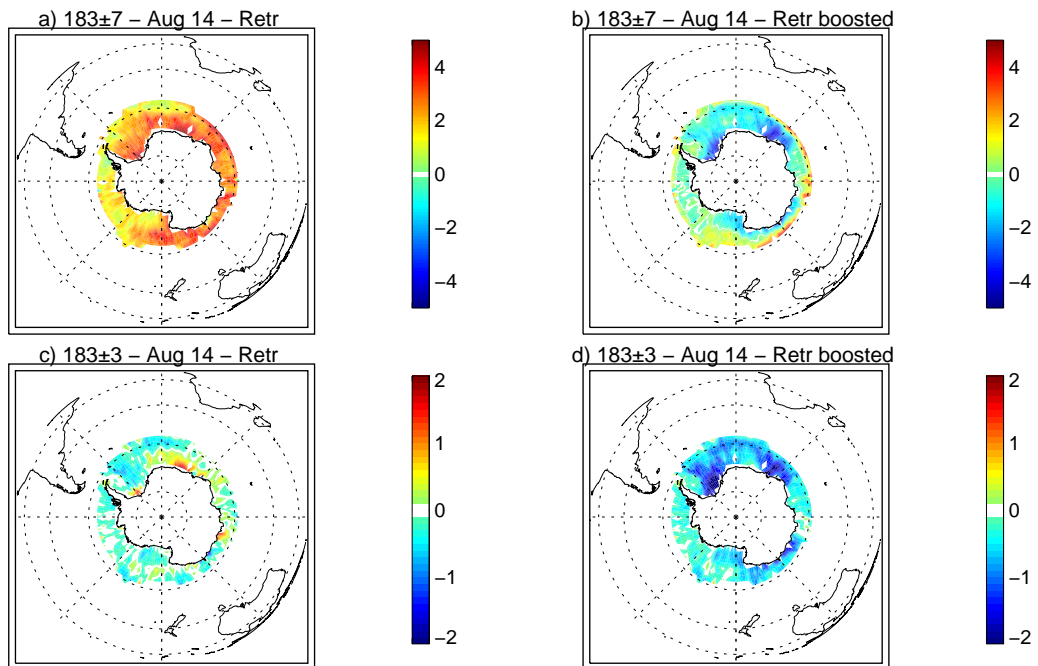
Figure 16: As Fig. 15, but for the winter (from 1 to 15 August 2014) in the Southern hemisphere.
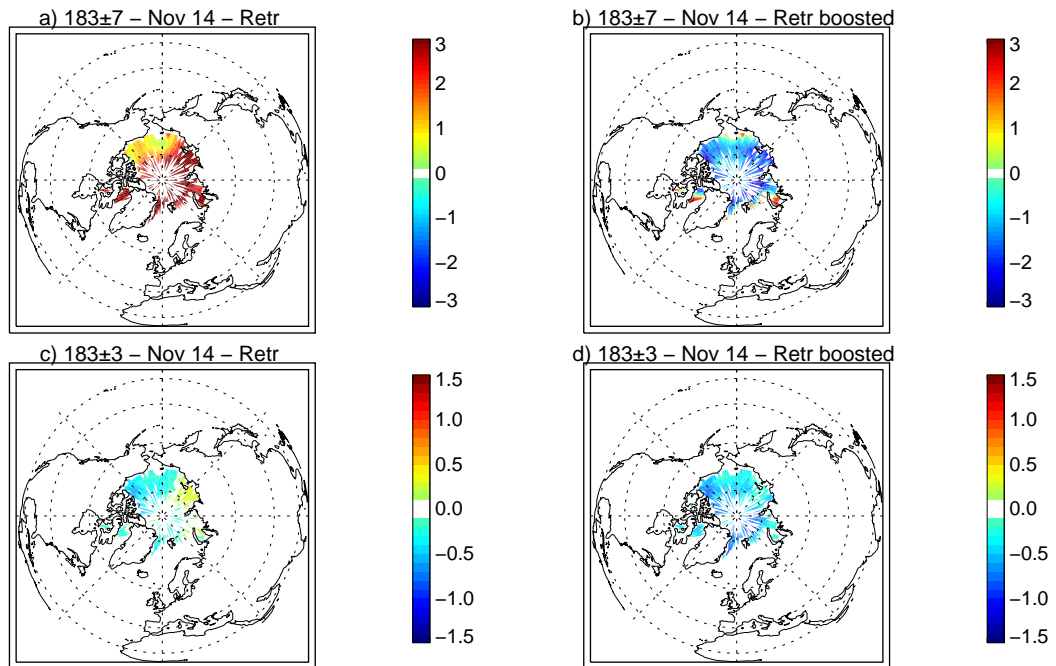
Figure 17: As Fig. 15, but for the autumn season (from 1 to 15 November 2014).
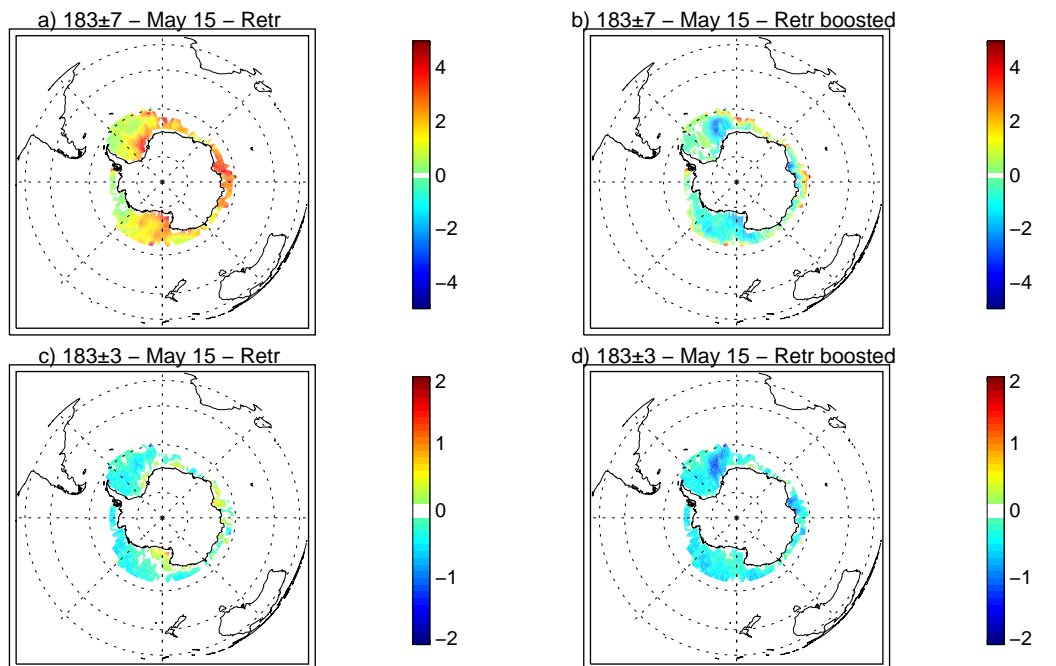

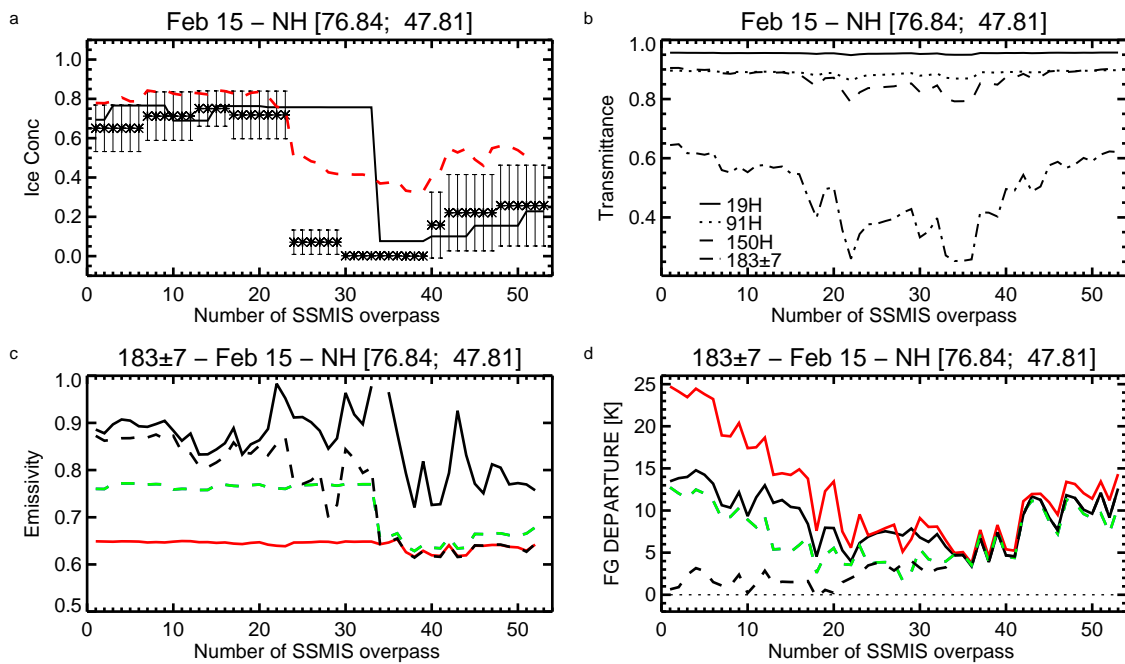*Figure 18: As Fig. 15, but for the autumn (from 1 to 15 May 2015) in the Southern hemisphere.*

Figure 19: Time series of data corresponding to SSMIS measurements in the Barents Sea (76.84°N; 47.81°E) from 1 to 15 February 2015 (for a total of 53 overpasses): **a)** *IFS sea-ice concentration (black line), mean (asterisk) and standard deviation (error bars) of OSI sea-ice concentration, and, as a reference, SSMIS emissivity retrievals at 19 GHz (dashed red line).* **b)** *Comparison of model transmittance across the 19-183 GHz range.* **c)** *Emissivity at 183±7 from the 'Retr' experiment (black line), the 'FYI' experiment (red line) and the two boosted experiment 'Retr boosted' (dashed black line) and 'FYI/MYI boosted' (dashed green line).* **d)** *First-guess departures at 183±7. Coloured lines are for different experiments as those in plot c.*

IFS C_{ice} is greater than 0.5 (overpasses between 1 and 34) the boost applied to the emissivity retrieval at 150 GHz generates a better fit to the observations (dashed black line). Improvements in the simulated brightness temperatures are also visible when the linear boost is applied to increase the FASTEM 'First' ice emissivity (dashed green line). Clearly the 'FYI' experiment, which uses the FASTEM emissivity at 183 GHz, is characterised by the lowest emissivity and the highest first guess departures (red line in Fig. 19 c and d). It is also very interesting to analyse what happens when the IFS C_{ice} decreases below 0.5 (overpasses between 35 and 53). In this case, the linear model is still applied to the 'FYI/MYI boosted' experiment, while the 'Retr boosted' experiment uses the FASTEM emissivity over ocean. As a result, the total emissivity over sea-ice in the 'FYI/MYI boosted' experiment, which is given by the weighted average of the ocean and ice emissivity, is characterised by a slight larger value (dashed green line Fig. 19 c). However, the emissivity appears to be still too low as demonstrated by the large positive first-guess departures of Fig. 19 d. This behaviour is not a deficiency in the linear model, but it is an indication that the IFS C_{ice} is probably too small and consequently the weight given to the ice emissivity is minimum. This highlights the importance of having also very accurate estimates of sea-ice concentration in order to improve the quality of the simulations and be capable of assimilating satellite data over sea-ice in NWP systems.

9   Conclusions

We explored the existing FASTEM parametric models to simulate microwave emissivity in order to evaluate the feasibility of being used for satellite data assimilation over sea-ice. To guide our analysis we used the ECMWF assimilation system in a configuration which allows us to only monitor the first-guess departures and we used the all-sky path which can process SSMIS data and also retrieve the surface emissivity directly from satellite observations. In our approach, when we use the FASTEM model, the emissivity over sea-ice surfaces is computed as the weighted average of the ocean and ice emissivity with weight given by the IFS sea-ice fraction. Results can be summarised as follows:

- Due to the high variability of the ice emissivity it is not feasible to adopt one single FASTEM ice model which can be globally used across all the 19-183 GHz range.

- For the 50-55 GHz range (e.g. temperature sounding channels), a single FASTEM emissivity (e.g. 'Compact' ice) could be used for simulating brightness temperature over sea-ice.

- We also found that the observed SSMIS gradient ratio (in agreement with the OSI product) might be a good predictor to cluster the surface and distinguish between the first-year and the multi-year ice. This appears to help the quality of the simulations in the Northern hemisphere, while in the South Pole it seems sufficient to categorise the surface only as first-year ice.

- Above 150 GHz and particularly at 183 GHz, FASTEM models cannot be used as they predict an estimate of emissivity that is too low. This is confirmed analysing SSMIS retrieved emissivities and first-guess departures. This is particularly important given that the 183 GHz channels are the only sea-ice sensitive channels being actively assimilated.

Through the relationship between the SSMIS retrievals at 183±7 and 150 GHz we built a simple model which can calculate the emissivity at 183 GHz as a linear function of the emissivity estimated at 150 GHz. The linear model was tested evaluating the impact on the first guess departures from different experiments. Results demonstrate that the boosting generally helps in reducing the large positive first-guess departures which are incorrectly generated when the FASTEM emissivity is used. However, results also show that it might be relevant to tune the linear model according to the season and geographical location.

The findings also suggest that it is critical to have a good estimate for the sea-ice concentration and it

might be possible to derive it from satellite observations directly in the NWP system. A good estimate and the capability of capturing daily changes in the sea-ice surface are two requirements which should be satisfied. This is something important to take into account for the current IFS/OSTIA sea-ice parameter which, for processing reasons, is characterised by a time-lag of up to one day in respect to the OSI product. The possibility of estimating the sea-ice concentration from satellite emissivity retrievals is briefly discussed in the Appendix.

To conclude, the use of the linear boost is generally promising and it might improve the satellite data assimilation of the humidity sounding channels over sea-ice. Data assimilation experiments will be run at ECMWF in order to evaluate the impact on SSMIS and MHS 183 GHz channels.

Acknowledgements

References

Aires F., Prigent C., Bernado F., Jimnez C., Saunders R. and Brunel P., 2010. A tool to estimate Land Surface-Emissivities at Microwaves frequencies (TELSEM) for use in numerical weather prediction. Q. J. R. Meteorol. Soc. 137, 690-699.

Baordo, F., Geer A.J. and English S., 2013. SSMI/S humidity sounding channels over land: second year EUMETSAT fellowship report. EUMETSAT/ECMWF Fellowship Programme Research Report No. 30, available from http://www.ecmwf.int.

Baordo, F. and Geer A.J., 2015. All-sky assimilation of SSMIS humidity sounding channels over land within the ECMWF system. To be submitted, Q.J.R. Meteorol. Soc.

Breivik, L.-A., Eastwood S., Godøy Ø., Schyberg H., Andersen S. and Tonboe R.T., 2001. Sea Ice Products for EUMETSAT Satellite Application Facility. Canadian Journal of Remote Sensing, Volume 27, No. 5.

Di Tomaso, E., Bormann, N. and English S., 2013. Assimilation of ATOVS radiances at ECMWF: third year EUMETSAT fellowship report. EUMETSAT/ECMWF Fellowship Programme Research Report No. 29, available from http://www.ecmwf.int.

Donlon, C. J., M. Martin, J. D. Stark, J. Roberts-Jones, E. Fiedler and W. Wimmer, 2011. The Operational Sea Surface Temperature and Sea Ice analysis (OSTIA). Remote Sensing of the Environment.

English S.J. and Hewison T.J., 1998. Fast generic millimeter-wave emissivity model. Proc. SPIE 3503, 288 (1998)

Geer A. J. and Bauer P. , 2010. Enhanced use of all-sky microwave observations sensitive to water vapour, cloud and precipitation. Published simultaneously as ECMWF Tech. Memo. 620 and ECMWF/EUMETSAT Fellowship Report No. 20, available from http://www.ecmwf.int.

Hewison T.J. and English S.J., 1999. Airborne Retrievals of Snow and Ice Surface Emissivity at Millimetre Wavelengths. IEEE Trans. Geosci.Remote Sensing, Vol.37, No.4, 1999, pp.1871-1879

Hewison, T.J., Selbach N., Heygster G., Taylor J.P. and McGrath A.J., 2002. Airborne Measurements of Arctic Sea Ice, Glacier and Snow Emissivity at 24-183 GHz. Proceedings of IGARSS 2002.
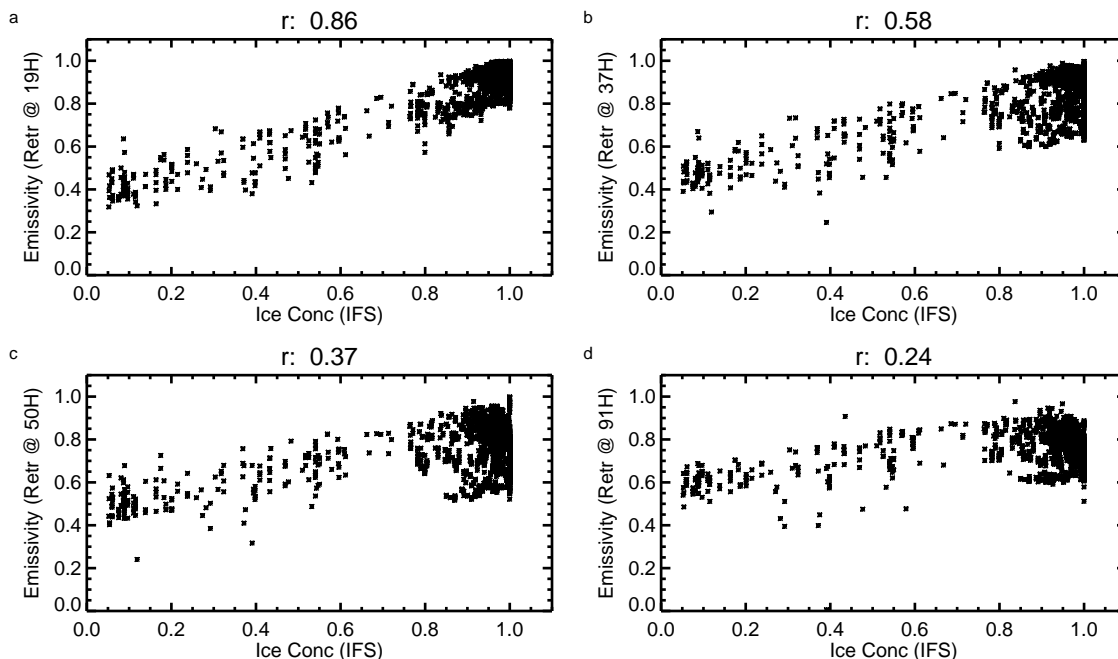
Figure 20: Relationship between the SSMIS emissivity retrievals at 19 (a), 37 (b), 50 (c) and 91 (d) GHz and the IFS sea-ice concentration. SSMIS observations are for the 1 February 2015 (from 9 to 21 UTC) in the North Pole. Pearson correlation coefficient (r) is also shown.

Hewison T.J., 2002. Analysis of emissivity data from POLEX: Initial results and Development of FASTEM for Arctic Surfaces. MRF Technical Note 35.

Karbou F., Prigent C., Eymard L. and Pardo J., 2005. Microwave land emissivity calculations using AMSUA and AMSU-B measurements. IEEE Trans. Geosci. Remote Sens. 46, 863-883.

Karbou F., Rabier F. and Prigent C., 2014. The Assimilation of Observations from the Advanced Microwave Sounding Unit over Sea Ice in the French Global Numerical Weather Prediction System. Mon. Wea. Rev., 142, 125-140.

Appendix: Sea-ice concentration from satellite emissivity retrievals

In this section we briefly discuss the possibility of estimating the sea-ice concentration from satellite emissivity retrievals. Due to the limited time, we were not able to evaluate an extensive number of case studies, but we simply looked at the sample of SSMIS observations taken the 1 February 2015 (from 9 to 21 UTC) over the Arctic Ocean. Results presented in this section are very promising and encourage additional studies to validate the methodology which has been used. Figure 20 explores the relationship between the SSMIS emissivity retrievals at 19, 37, 50 and 91 GHz and the IFS sea-ice concentration. Results are clearly in favour of the lower frequencies and the retrievals at 19 GHz present the highest degree of correlation (0.86). The first option we explored to estimate the sea-ice fraction from the emissivity retrievals is simply to resolve Eq. 1 for C_{ice}. This gives (we omit the dependency on the frequency ν and the incidence angle θ):

$$C_{ice} = \frac{\varepsilon_{retr} - \varepsilon_{ocean}}{\varepsilon_{ice} - \varepsilon_{ocean}}. \tag{4}$$
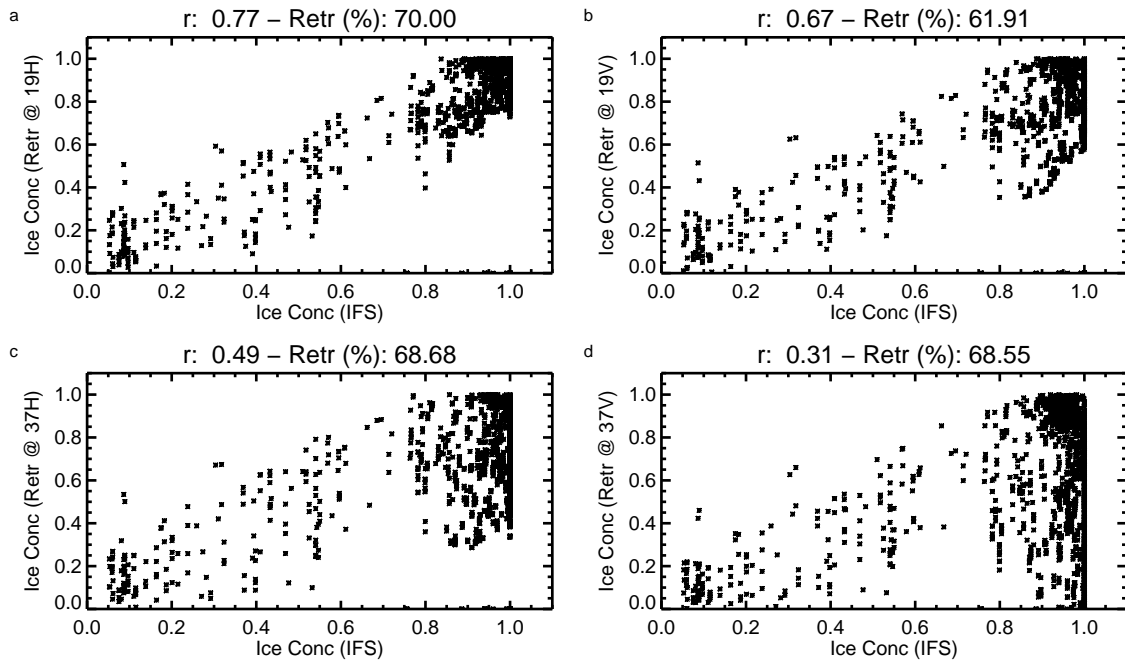
Figure 21: Relationship between the sea-ice concentration retrieved from SSMIS emissivity at 19H (a), 19V (b), 37H (c), 37V (d) and the IFS sea-ice concentration. Plots also shown the Pearson correlation coefficient (r) and the percentage of successful retrievals (sea-ice concentration between 0 and 1).

For a fixed frequency, C_{ice} can be directly calculated from the emissivity estimated by satellite observations and from the emissivities provided by the FASTEM model respectively over ocean and ice. In the calculations presented below, the ice emissivity has been always considered as that from the FASTEM 'First' ice category. From Eq. 4 we derived the C_{ice} only taking into account the 2 lower frequencies 19 and 37 GHz which, as previously demonstrated, are those characterised by retrievals more correlated with the sea-ice fraction. Figure 21 (a, b, c and d) shows the ice concentrations derived respectively from 19H, 19V, 37H and 37V as a function of the IFS C_{ice}. Every plot also provides the Pearson correlation coefficient and the percentage of successful retrievals (sea-ice concentration between 0 and 1). The use of the emissivity retrievals at 19H generates the best results (highest correlation and largest number of sea-ice concentration retrievals). For the 19H case, we also analyse the number of successful and unsuccessful sea-ice fraction retrieval through polar stereographic maps. Figure 22 b and d compare respectively the successful and unsuccessful retrievals to those from the IFS, Figure 22 a and c. The sample of successful retrievals seems to be slightly lower compared to the IFS estimates. The unsuccessful retrievals, instead, are slightly larger than 1 and, considering the equivalent sample of IFS data, it might be reasonable to accept these retrievals and assign them a sea-ice fraction equal to 1. This assumption is explored in Fig. 23 which compares the full set of the sea-ice retrievals (including values larger than 1) respectively to those from the IFS (Fig. 23 a) and the OSI product (Fig. 23 b). The correlation between retrievals and OSI sea-ice concentration is larger: this result confirms that, as previously discussed for the Barents Sea case study, the IFS parameter might not efficiently capture daily changes in the sea-ice surfaces.

The second method we investigated is based on the possibility of deriving the estimate of the sea-ice fraction using simultaneous emissivity retrievals at a number of frequencies through a multiple linear regression. Eq. 1 can be reformulated in the following way:
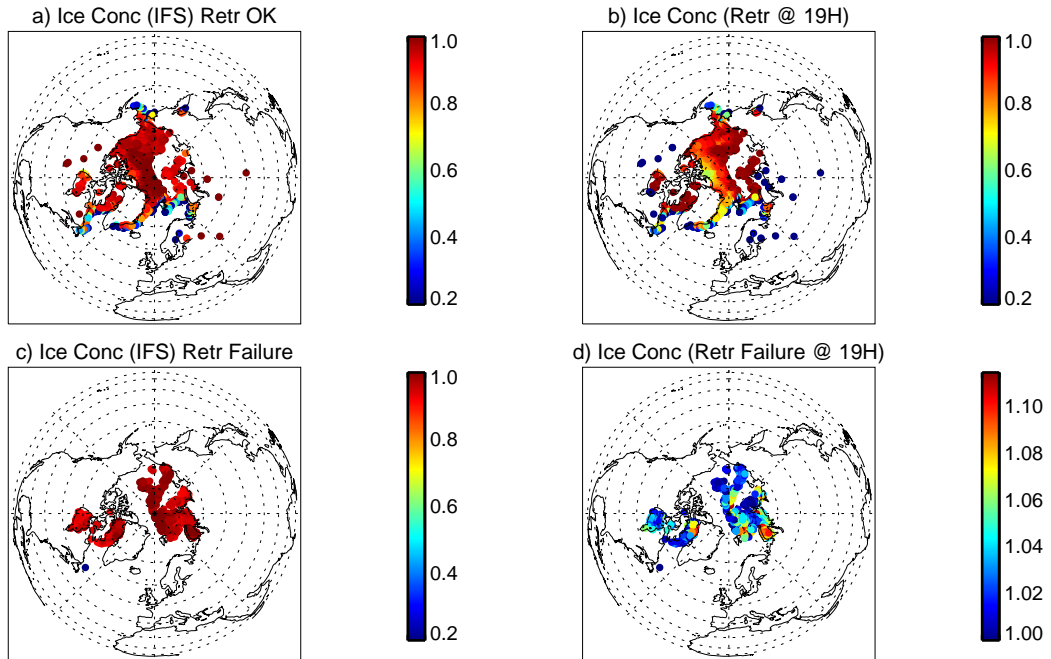
Figure 22: Polar stereographic maps of successful (b) and unsuccessful (d) sea-ice concentration retrievals using SSMIS emissivity at 19H compared respectively to equivalent sample of sea-ice concentration from IFS (a and c).
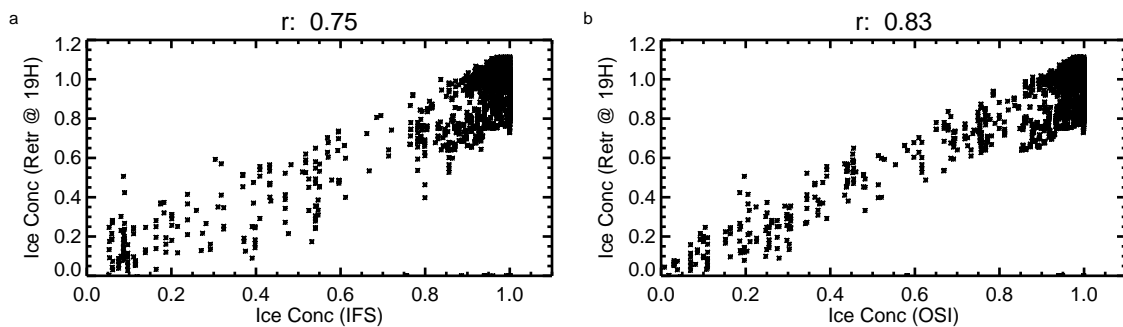

Figure 23: As Fig. 21 a, but also considering those retrievals of sea-ice concentration greater than 1. Retrievals are separately plotted as a function of the IFS C_{ice} (a) and the OSI product (b). Pearson correlation coefficient (r) is also shown.

$$Y = mX + q, \tag{5}$$

where

$$Y = \frac{\varepsilon_{retr}}{\varepsilon_{ocean}},$$
$$X = \frac{\varepsilon_{ice}}{\varepsilon_{ocean}},$$
$$m = C_{ice},$$
$$q = C_{water} = 1 - C_{ice}.$$

In our approach Y and X are vectors with size given by the number of frequencies for which emissivity retrievals are considered. In our case study we found that the use of 19H, 19V, 37H and 37V gives the best results. However, we cannot exclude that the use of more frequencies might be beneficial in other situations. The ambiguity of the linear regression is that the sea-ice concentration can be equally estimated from m and q and in the IDL regression function we used there is no possibility to properly constrain the solution for the coefficients (in our case should be $m + q = C_{ice} + C_{water} = 1$). This ambiguity is explored in Fig. 24 which shows the sea-ice concentration retrieved from both m and q as a function of the IFS sea-ice concentration. As for Fig. 21, Fig. 24 provides the Pearson correlation coefficient (r) and the percentage of successful retrievals. Results show that we obtain better results when the C_{ice} is estimated from the coefficient m (Fig. 24 a). Comparing Fig. 24 a with Fig. 21 a we can infer that the multi-frequency approach largely improves the correlation coefficient although the number of successful retrievals is reduced of about 11%. Polar stereographic maps can again be used to explore the number of successful and unsuccessful retrievals (Fig. 25). The linear regression approach through the coefficient m is actually improving the C_{ice} retrievals which are closer in value to those of IFS (Fig. 25 a and b). Although the number of unsuccessful retrievals is larger, as in the single frequency approach, they are characterised by a value slightly larger than 1 (Fig. 25 d) which might be reasonably accepted as 1. As previously done, Fig. 26 compares the full set of the sea-ice retrievals (including also values larger than 1) respectively to those from the IFS (Fig. 26 a) and the OSI product (Fig. 26 b). Also in this case, the correlation between retrievals and OSI sea-ice concentration is higher and, overall, the use of the multiple linear regression approach increases the correlation of 11% compared to the case when the single frequency method is used (Fig. 23 b versus Fig. 26 b). To conclude, the multi-frequency approach is definitely promising and it should be investigated further in the future. For our initial exploration we have used a single ice category (FASTEM 'First'), but the use of multiple ice models might also provide additional improvements.
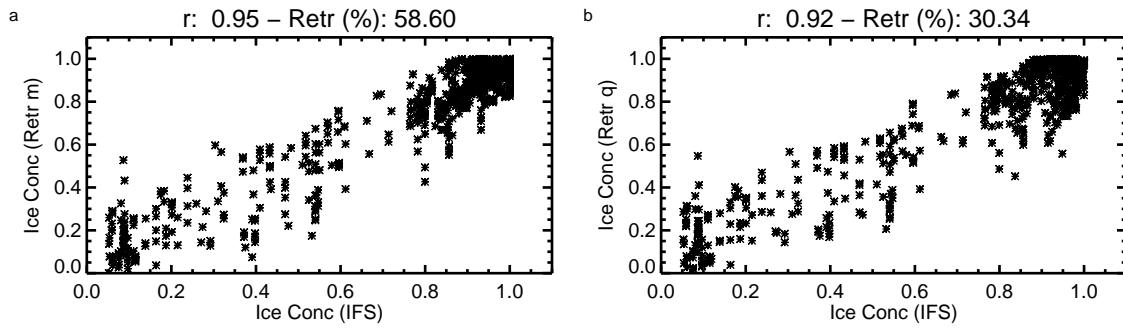
Figure 24: Relationship between the sea-ice concentration retrieved from the coefficients of he linear regression m (a) and q (b) and the IFS sea-ice concentration. Plots also shown the Pearson correlation coefficient (r) and the percentage of successful retrievals (sea-ice concentration between 0 and 1).
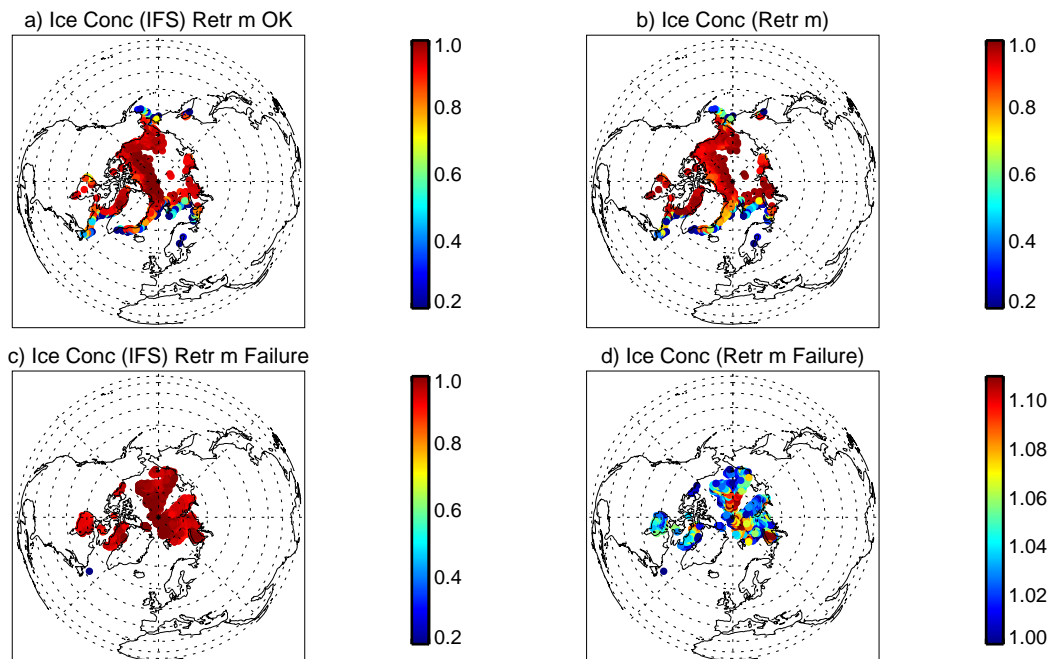

Figure 25: Polar stereographic maps of successful (b) and unsuccessful (d) sea-ice concentration retrievals from the coefficient m of the linear regression compared respectively to equivalent sample of sea-ice concentration from IFS (a and c).
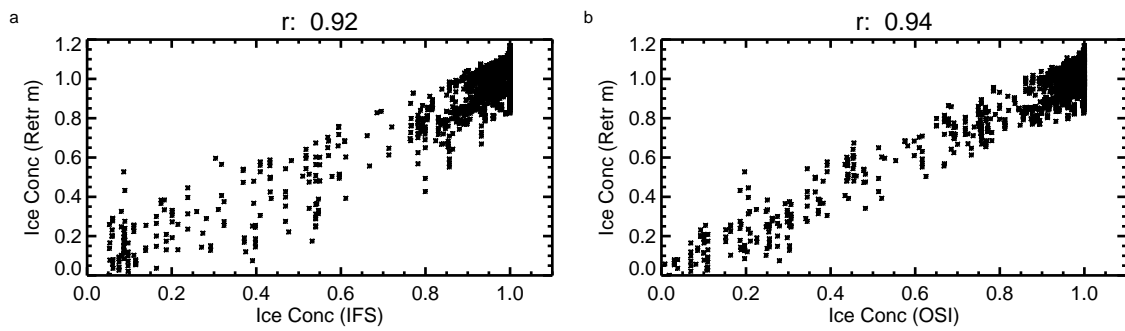
Figure 26: As Fig. 24 a, but also considering those retrievals of sea-ice concentration greater than 1. Retrievals are separately plotted as a function the IFS C_{ice} (a) and the OSI sea-ice fraction (b). Pearson correlation coefficient (r) is also shown.